Acta Geotechnica (2024) 19:6195–6216
https://doi.org/10.1007/s11440-024-02297-w

RESEARCH PAPER

Probability-based analyses of bearing capacity of square and rectangular footings resting on sandy soil considering rotational anisotropy

Kouseya Choudhuri[1] · Debarghya Chakraborty[1]

Received: 17 March 2023 / Accepted: 6 February 2024 / Published online: 26 March 2024

Abstract
The present study explores the effect of rotational anisotropy on the bearing capacity responses of the square and rectangular footings using the random finite difference method (RFDM) and Monte Carlo simulation (MCS) technique. Three different aspect ratios (i.e., L/B = 1, 2, and 3) are considered in this study. The lognormal distribution is chosen for the spatial distribution of the tangent of the friction angle. The probabilistic bearing capacity response (μN_γ) and the failure probability (p_f) of the footings are obtained for different angles of rotation of the soil strata (β) considering different orientations of the footings. The probabilistic results are presented in the form of *PDF* and *CDF* for different β and L/B ratios of the footing. The desired safety factors (FS_r) corresponding to a specific target failure probability (say p_{ft} = 0.01%) are also evaluated for different β. It is found that the orientation of the rectangular footings with respect to the strike direction of the soil strata has significant effects on the μN_γ and p_f of the footings.

Keywords Desired safety factor · Monte Carlo realizations · Orientations of the rectangular footings · Rotational anisotropy · Three-dimensional footings

1 Introduction

In usual practice, most geomechanics problems are analyzed using the deterministic approach, where the soil is assumed to be either a single layer with homogeneous and uniform properties or a multilayer with layer-wise homogeneous and uniform properties. The factor of safety concept is incorporated to ensure the safety of the structure. However, due to the complex geological processes (like the formation of the soil matrix, deposition and decomposition processes, different loading or stress histories, tectonic movements, etc.), the soil properties tend to vary in space. Over the last two decades, researchers have incorporated the spatial variability concept in their study to achieve the realistic and economical design of geotechnical structures. These studies include the ultimate bearing capacity of the footings [2, 5, 11, 13, 16, 17, 19, 30, 32, 33, 35, 37, 43], the ultimate bearing capacity of offshore strip footings [36, 44, 45, 47, 48], settlement analysis of footings [1, 12, 14, 20], footing on the slope [10, 25, 39, 49, 50], slope stability analysis [9, 18, 21, 31, 34], laterally loaded pile [24], braced excavation [38] and so forth. All these studies above were analyzed considering either isotropic random field (where the scales of fluctuation or autocorrelation lengths in both horizontal and vertical directions are the same) or transverse horizontal anisotropic random field (where the scale of fluctuation or autocorrelation length in the vertical direction is relatively less than that for the horizontal direction). In the case of a transverse horizontal anisotropy, due to the natural soil deposition process, the rate of changes in the soil properties along the horizontal direction is comparatively less than that along the vertical direction. Hence, the horizontal scale of fluctuation or autocorrelation length is higher than that for the vertical direction for transverse horizontal anisotropy. However, due to the tectonic movements and different

✉ Debarghya Chakraborty
debarghya@civil.iitkgp.ac.in

Kouseya Choudhuri
kousheyo1995@iitkgp.ac.in

[1] Department of Civil Engineering, Indian Institute of Technology, Kharagpur, India

geological mechanisms forming the complex soil structure, the variability of the soil properties may differ from the isotropic and transverse horizontal anisotropic fields [28, 40]. Zhu and Zhang [52] classified heterogeneity into three different types (along with isotropy and transverse anisotropy), which are rotated anisotropy, general anisotropy, general rotated anisotropy, and the combinations of these different types of heterogeneity. Several studies [4, 22, 26, 27, 53] are available on the two-dimensional slope stability analyses considering the spatially variable random field of rotated anisotropy. The rotated anisotropy case is a special case of transverse anisotropy where the two mutually perpendicular principal axes (major and minor principal axes) of the scale of fluctuation or autocorrelation length are rotated by an angle of β with respect to the horizontal direction. The angle β is called the angle of rotation of the soil strata.

In the study of Griffiths et al. [22], two types of failure mechanisms were proposed, which are series and parallel failure mechanisms. In the case of the series failure mechanism, the orientation of the strata is parallel to the slope (known as the dip slope). Consequently, a significant portion of the failure surface is parallel to the strata orientation (refer to Fig. 1a). However, in the case of the parallel failure mechanism, the orientation of the strata is perpendicular to the slope (known as the reverse-dip slope). The failure surface passes through the alternate strong and weak soil layers (refer to Fig. 1b). It was reported that the series failure mechanism provides a higher failure probability than the parallel failure mechanism. Considering the rotated anisotropy, Cheng et al. [7] used the RFDM to evaluate the risk associated with slope failure. It was found that depending upon the rotation angle of the strata, rotated anisotropy provides both shallow and deep failure mechanisms as compared to horizontal transverse anisotropy. Zhu et al. [53] reported in their study that the minimum safety factor is obtained for the strata rotation angle of 30^{o}, which is lower than the slope angle. Huang and Leung [28] conducted a three-dimensional reliability-based slope stability analysis using the random finite element method (RFEM), considering the rotational anisotropy, where the strata rotation has been considered around the three coordinate axes. It was observed that the cross-dip and the reverse-dip slope could be considered desirable slope stability conditions as compared to the dip slope.

All the above studies considering rotational anisotropy were restricted to slope stability analyses. However, considering the rotational anisotropy of the soil strata, the bearing capacity analyses of the footing are very limited. Ghazavi et al. [15] carried out the probabilistic plane strain analysis of a strip footing resting on the top of rotated anisotropic cohesive-frictional soil underlain by bedrock incorporating the RFDM. The effects of the angle of rotation of the soil strata and the angle of bedrock inclination were also explored in their study. Luo and Luo [40] investigated the effect of rotational anisotropy of the undrained shear strength on the ultimate bearing capacity of an embedded strip footing, considering plane strain conditions under the RFEM framework. It was observed from their study that the mean ultimate bearing capacity remains constant irrespective of the change in the rotation angle of the strata, whereas the failure probability increases as the rotation angle of the strata increases. Luo and Luo [41] explored the effect of rotated anisotropy on the performance of a two-dimensional strip footing located on the edge of a slope utilizing the RFEM. It was reported that the variability associated with the footing bearing capacity, sliding mass, failure probability, and the associated risks are at a peak when the strata orientation is parallel to the slope inclination.

All the above literature shows that no probability-based study exists for the bearing capacity analysis of the three-dimensional footings (like square, rectangular, etc.) considering rotated soil anisotropy. Hence, the present study aims to explore the effect of rotational anisotropy on the bearing capacity and failure mechanisms of the three-dimensional square and rectangular footings resting on the top of a spatially variable granular soil under the random

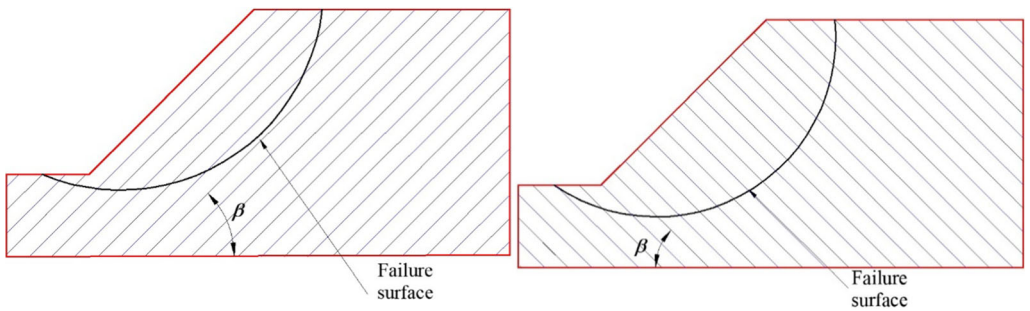

Fig. 1 Failure mechanisms. **a** Series, **b** Parallel

finite difference framework. Although the probabilistic analyses of three-dimensional footings are computationally expensive, it is essential to study them as they are constructed to carry massive super-structural loads, and the risk correlated with the failure of the system needs to be properly assessed [11, 32]. The present study assumes the tangent of friction angle (i.e., tan ϕ) as the spatially variable random field following the lognormal distribution. Three different typical conditions are considered in the present study: (1) square footing under rotational anisotropy (refer to Fig. 2a), (2) rectangular footing under rotational anisotropy where the length direction of the footing is parallel to the strike direction of the soil strata orientation (refer to Fig. 2b), and (3) rectangular footing under rotational anisotropy where the length direction of the footing is perpendicular to the strike direction of the soil strata orientation (refer to Fig. 2c). The obtained bearing capacity of the footings is represented using the dimensionless bearing capacity factor (N_γ), which can be evaluated using the following equation:

$$N_\gamma = \frac{q_{\text{ult}}}{0.5\gamma B} \tag{1}$$

where q_{ult} is the ultimate bearing capacity of the footing, B is the width of the footing, and γ is the unit weight of the soil. The ultimate bearing capacity of the footing (q_{ult}) is evaluated using the following equation:

$$q_{\text{ult}} = \frac{Q_{\text{c}}}{A} \tag{2}$$

where Q_c is the collapse load applied on the footing, and A is the base area of the footing. Before executing the probabilistic analyses, the deterministic analysis of the footings is carried out, considering the soil parameters to be uniform and homogeneous all over the soil domain. In the case of probabilistic analyses, only a single value has been considered for the coefficient of variation of tan ϕ ($COV_{\tan\phi}$), major and minor scales of fluctuation (θ_{mj} and θ_{mn}), while the angle of rotation of the strata (β) is the subject of the parametric study. The Monte Carlo simulation technique is incorporated to find out the mean bearing capacity factor (μN_γ) and failure probability (p_f) of the square and rectangular footings corresponding to different angles of rotation of the strata (β). The *CDF* and *PDF*

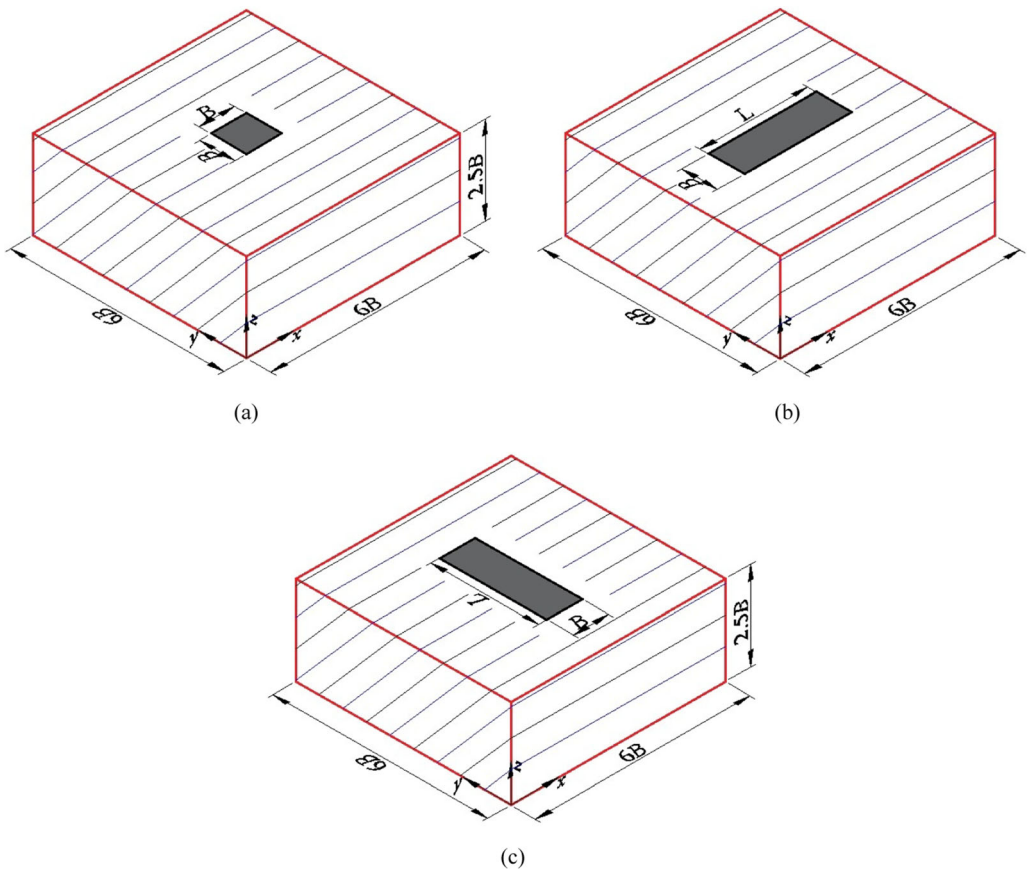

Fig. 2 Schematic diagram of **a** square footing under rotational anisotropy, **b** rectangular footing under rotational anisotropy where length (L) direction is parallel to strike **c** rectangular footing under rotational anisotropy where length (L) direction is perpendicular to strike

curves are plotted for different β, and the desired safety factors (FS_r) are obtained for different β corresponding to a specific target failure probability (p_{ft}).

2 Details of the finite-difference modeling

The explicit finite-difference software FLAC^{3D} [29] was used to execute both the deterministic and probabilistic analyses of the problem. The square and rectangular footings (having B = 1 m) were considered to be rough and rigid, resting on the surface of the granular soil deposit. The soil domain of the model was considered as 6B in both the horizontal directions (i.e., in the x and y directions) and 2.5 B in the vertical direction (i.e., in the z-direction). The bottom of the soil model was restricted in all three directions, whereas the side boundaries were restricted in the lateral direction to allow the model to displace only in the vertical direction. The eight-node brick-shaped elements were used to discretize the whole soil model, and the uniform mesh was generated throughout the study. The total number of elements was considered to be 46,080. The domain and mesh sizes chosen for this problem were taken after several trials to maintain the balance between efficiency and accuracy. The domain and the mesh convergence studies for the rectangular footing having L = 3B are presented in Table 1a and b based on deterministic analysis. The granular soil deposit was assumed to follow the Mohr–Coulomb yield criterion. In this study, the elastic modulus (E) and Poisson's ratio (υ) of the granular soil were considered to be 20 MPa and 0.3, respectively (following Bowels [4]). The unit weight of the soil (γ) was assumed as 20 kN/m^3. After discretizing the whole soil domain, the soil properties were allocated to each finite-difference mesh grid. Then, the gravity analysis was done for the whole model. After the gravity analysis, the settlement of the whole domain was set to zero. The footing roughness was ensured by providing lateral resistance to the nodes representing the footing area. An optimal downward velocity of magnitude 1×10^{-5} m/step was applied to the footing nodes to determine the bearing capacity-settlement response. The discretized mesh with a rectangular footing (L/B = 3) is illustrated in Fig. 3.

3 Deterministic analysis

Before executing the probabilistic analyses, the deterministic analyses were carried out for the square and rectangular footings to find the benchmark value of N_γ (i.e., N_{γ_det}) for the probabilistic analyses and evaluate the failure probability (p_f) of the system. In the deterministic analyses, non-random uniform and homogeneous soil properties were allocated to all the finite-difference grids. The soil friction angle (ϕ) and the corresponding dilation angle (ψ) were assumed to be 30^o and 0^o, respectively, for the analyses. The bearing pressure-settlement response of the square (L/B = 1) and rectangular footings (L/B = 2 and L/B = 3) are obtained and illustrated in Fig. 4. The q_{ult} was considered as the bearing pressure corresponding to the settlement ratio (footing settlement normalized to the width of the footing, s/B) of 6% as the change in bearing pressure value with respect to the s/B is marginal beyond s/B = 6%. Moreover, as per Eurocode 7 [3], the maximum allowable settlement for the typical footings for sand is 50–75 mm, and the settlement value of 6% of B was within the prescribed range. Hence, the settlement-based criterion was also taken into consideration to define the q_{ult}. The N_{γ_det}

Table 1 (a) Domain effect and (b) Mesh convergence study

The aspect ratio of the footing	The extent of the boundary	Number of elements	N_γ	% Difference
(a) Domain effect study				
L/B = 3	6 x 6× 2.5 m	46,080	20.04	–
	6 x 6 x 3 m	55,296	20.018	0.11
	6 x 6 x 4 m	73,728	19.966	0.37
	7 x 7 x 3 m	75,264	19.940	0.50
	7 x 7 × 3.5 m	87,808	19.899	0.70
	7 x 7 x 4 m	100,352	19.797	1.21
	8 x 8 x 4 m	131,072	19.696	1.72
(b) Mesh convergence study				
L/B = 3	6 x 6 × 2.5 m	5760	23.65	18.46
		19,440	21.40	7.21
		46,080	20.04	0.26
		90,000	19.96	–

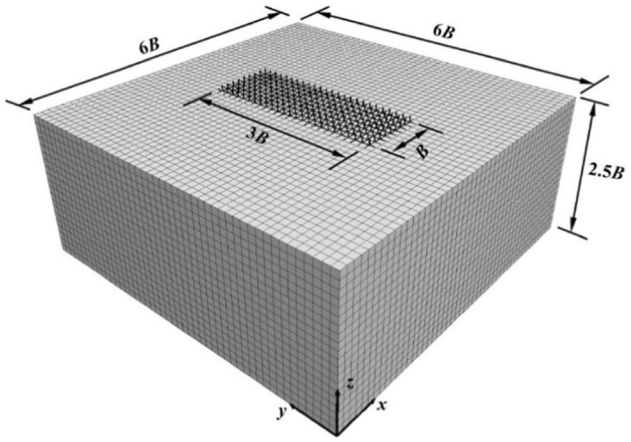

Fig. 3 Finite-difference discretization of the soil domain with a rectangular surface footing (L/B = 3)

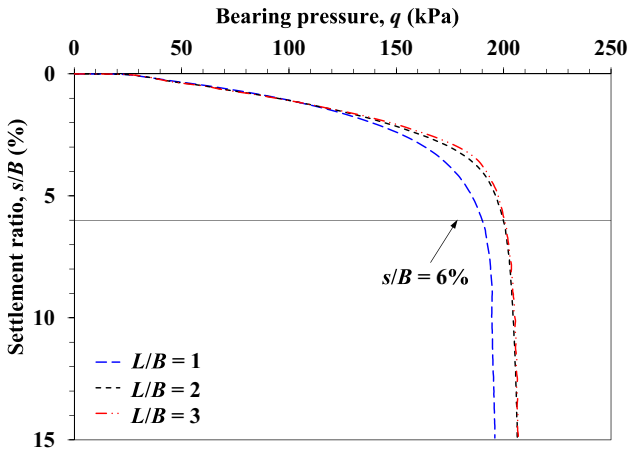

Fig. 4 Bearing pressure-settlement response for footings with the different aspect ratios

value was obtained based on the ultimate bearing capacity (q_{ult}) value. The values of N_{γ_det} for the footings with different aspect ratios are provided in Table 2. It was found that the N_{γ_det} value increased with the increase in footing size. However, the difference between N_{γ_det} values for L/B = 2 and L/B = 3 was very marginal.

4 Probabilistic analysis

4.1 Autocorrelation matrix formulation

Due to the different complex geological processes, the soil properties tend to vary in space. In general cases, the horizontal stratification of the soil profile is observed in nature because of the soil deposition process. However, geologic faults are created due to tectonic movements, which may cause rotational anisotropy in the soil profile. In horizontal transverse anisotropy for three-dimensional analysis, the scales of fluctuation in both horizontal directions are assumed to be the same, i.e., $\theta_x = \theta_y$ [11, 32], and the vertical scale of fluctuation (θ_z) is lower than the $\theta_x = \theta_y$. In contrast to the three-dimensional analysis, the scale of fluctuation in the out-of-plane direction is infinite for the two-dimensional plane strain analysis (i.e., $\theta_y = \infty$). Hence, the results obtained for the two-dimensional plane strain analysis (i.e., $\theta_x > \theta_z$; $\theta_y = \infty$) are lower than those for the three-dimensional analysis (i.e., $\theta_x = \theta_y > \theta_z$) considering the identical statistical parameters (mean, *COV*, scale of fluctuation). The reason behind this can be attributed to the absence of the averaging effect in the out-of-plane direction for the plane strain analysis [8, 50]. Therefore, the results corresponding to the two-dimensional probabilistic analysis are underestimated, which may be unrealistic during the design of the structure. In the case of rotational anisotropy, the Cartesian coordinate system is rotated by an angle β, and the major scale of fluctuation (θ_{mj}) corresponds to the horizontal scale of fluctuation ($\theta_x = \theta_y$) and the minor one (θ_{mn}) to the vertical scale of fluctuation (θ_z). Thus, the three-dimensional autocorrelation structure for rotational anisotropy can be obtained from the autocorrelation structure for horizontal transverse anisotropy by transforming the coordinate system [28, 50]. The autocorrelation structure for the rotational anisotropy considering the rotation of the soil strata can be expressed using the following expression [28]:

Table 2 Deterministic N_{γ_det} values for the footings with the different aspect ratios

The aspect ratio of the footing	N_{γ_det}		
	Present study	Zhu and Michalowski [47]	
		Finite element method	Closed-form expression
L/B = 1	19.01	18.309 (3.69%)	18.703 (1.62%)
L/B = 2	19.99	19.687 (1.52%)	19.195 (3.98%)
L/B = 3	20.04	19.884 (0.78%)	19.358 (3.40%)

$$\rho = \exp\left[-2\sqrt{\left(\frac{\tau_x}{\theta_{\mathrm{mj}}}\right)^2 + \left(\frac{\tau_y \cos\beta + \tau_z \sin\beta}{\theta_{\mathrm{mj}}}\right)^2 + \left(\frac{-\tau_y \sin\beta + \tau_z \cos\beta}{\theta_{\mathrm{mn}}}\right)^2}\right] \tag{3}$$

In the above equation, $\tau_x = (x_k - x_l)$, $\tau_y = (y_k - y_l)$, and $\tau_z = (z_k - z_l)$ are the distances between the centroids of k^{th} and l^{th} elements, where k = 1, 2, 3, …, E_n, and l = 1, 2, 3, …, E_n (E_n is the total number of elements in the generated mesh). θ_{mj} is the major scale of fluctuation, and θ_{mn} is the minor scale of fluctuation. β is the angle of rotation of the soil strata. Using the autocorrelation structures evaluated in Eq. (3), the autocorrelation matrix (A) can be formulated as follows:

$$A = \begin{bmatrix} 1 & \rho(\tau_{x12}, \tau_{y12}, \tau_{z12}) & \rho(\tau_{x13}, \tau_{y13}, \tau_{z13}) & \cdots & \rho(\tau_{x1E_n}, \tau_{y1E_n}, \tau_{z1E_n}) \\ \rho(\tau_{x21}, \tau_{y21}, \tau_{z21}) & 1 & \rho(\tau_{x23}, \tau_{y23}, \tau_{z23}) & \cdots & \rho(\tau_{x2E_n}, \tau_{y2E_n}, \tau_{z2E_n}) \\ \rho(\tau_{x31}, \tau_{y31}, \tau_{z31}) & \rho(\tau_{x32}, \tau_{y32}, \tau_{z32}) & 1 & \cdots & \rho(\tau_{x3E_n}, \tau_{y3E_n}, \tau_{z3E_n}) \\ \vdots & \vdots & \vdots & \ddots & \vdots \\ \rho(\tau_{xE_n1}, \tau_{yE_n1}, \tau_{zE_n1}) & \rho(\tau_{xE_n2}, \tau_{yE_n2}, \tau_{zE_n2}) & \rho(\tau_{xE_n3}, \tau_{yE_n3}, \tau_{zE_n3}) & \cdots & 1 \end{bmatrix}_{E_n \times E_n} \tag{4}$$

4.2 Random field generation for friction angle (ϕ)

The present study characterized the tangent of friction angle (tan ϕ) as a lognormally distributed random field. The tangent of ϕ was considered as a random field instead of ϕ as the generated ϕ values are always positive and fall within the range of 0° and 90° [10, 23, 33]. The study assumed the dilation angle (ψ) as a non-random parameter. After evaluating the autocorrelation matrix (A), the Cholesky decomposition method was used for the random field generation, following the literature [15, 28, 52]. Since the obtained autocorrelation matrix is positive definite, the matrix can be decomposed into the lower triangular matrix (L) and its transpose (L^T) given as follows:

$$A = LL^{\mathrm{T}} \tag{5}$$

The correlated standard normal random field for tan ϕ ($\overline{G}$) can be evaluated using the lower triangular matrix (L) obtained from Eq. (6) as follows:

$$\overline{G} = \sum_{j=1}^{i} L_{ij} G_j \quad ; i = 1, 2, 3, \ldots, E_{\mathrm{n}} \tag{6}$$

where G denotes the column vector of the uncorrelated standard normal variable with zero mean and unit standard deviation. Hence, the spatially varied random fields for ϕ can be expressed as follows:

$$\phi(\xi) = \tan^{-1}[\exp(\mu_{\ln\tan\phi} + \sigma_{\ln\tan\phi}\overline{G})] \tag{7}$$

In the above equation, $\xi = \xi(x, y, z)$ denotes the spatial location of a point where the friction field is required. The normal distribution parameters $\mu_{\ln\tan\phi}$ and $\sigma_{\ln\tan\phi}$ were evaluated using the following transformations:

$$\sigma^2_{\ln\tan\phi} = \ln\left(1 + \frac{\sigma^2_{\tan\phi}}{\mu^2_{\tan\phi}}\right) = \ln(1 + COV^2_{\tan\phi}) \tag{8}$$

$$\mu_{\ln\tan\phi} = \ln\mu_{\tan\phi} - \frac{1}{2}\sigma^2_{\ln\tan\phi} \tag{9}$$

To extract the centroidal coordinates of all the elements of the discretized soil domain as a text file, an in-house FISH subroutine was written in FLAC^{3D}. After extracting those coordinates into the text files, the files were loaded into MATLAB [46]. The spatially varied random field for ϕ was generated in MATLAB using the probabilistic parameters provided in Table 3. Then the obtained random fields were taken back to FLAC^{3D} as the text file and assigned to each element of the discretized mesh using the FISH subroutine. The exemplary random fields of ϕ for different β are illustrated in Fig. 5. It is to be noted that the illustrated random fields corresponded to a particular Monte Carlo realization.

Table 3 Probabilistic parameters used in the present study

Parameters	Values
Mean of tangent of friction angle, $\mu_{\tan\ \phi}$	tan (30°)
Coefficient of variation of the tangent of friction angle, $COV_{\tan\phi}$	15%
Major scale of fluctuation, θ_{mj}/B	10
Minor scale of fluctuation, θ_{mn}/B	1
Angle of rotation of the soil strata, β	0°, 15°, 30°, 45°, 60°, 75°, 90°

4.3 Monte Carlo simulation (MCS)

The μN_γ and COV_N_γ for the given sets of probabilistic parameters were evaluated using the MCS technique. In spite of having identical probabilistic statistics of soil friction angle, different spatial distributions of ϕ are expected for different Monte Carlo (MC) realizations. Hence, the different probabilistic N_γ values are most likely to be obtained for different MC realizations. It should be

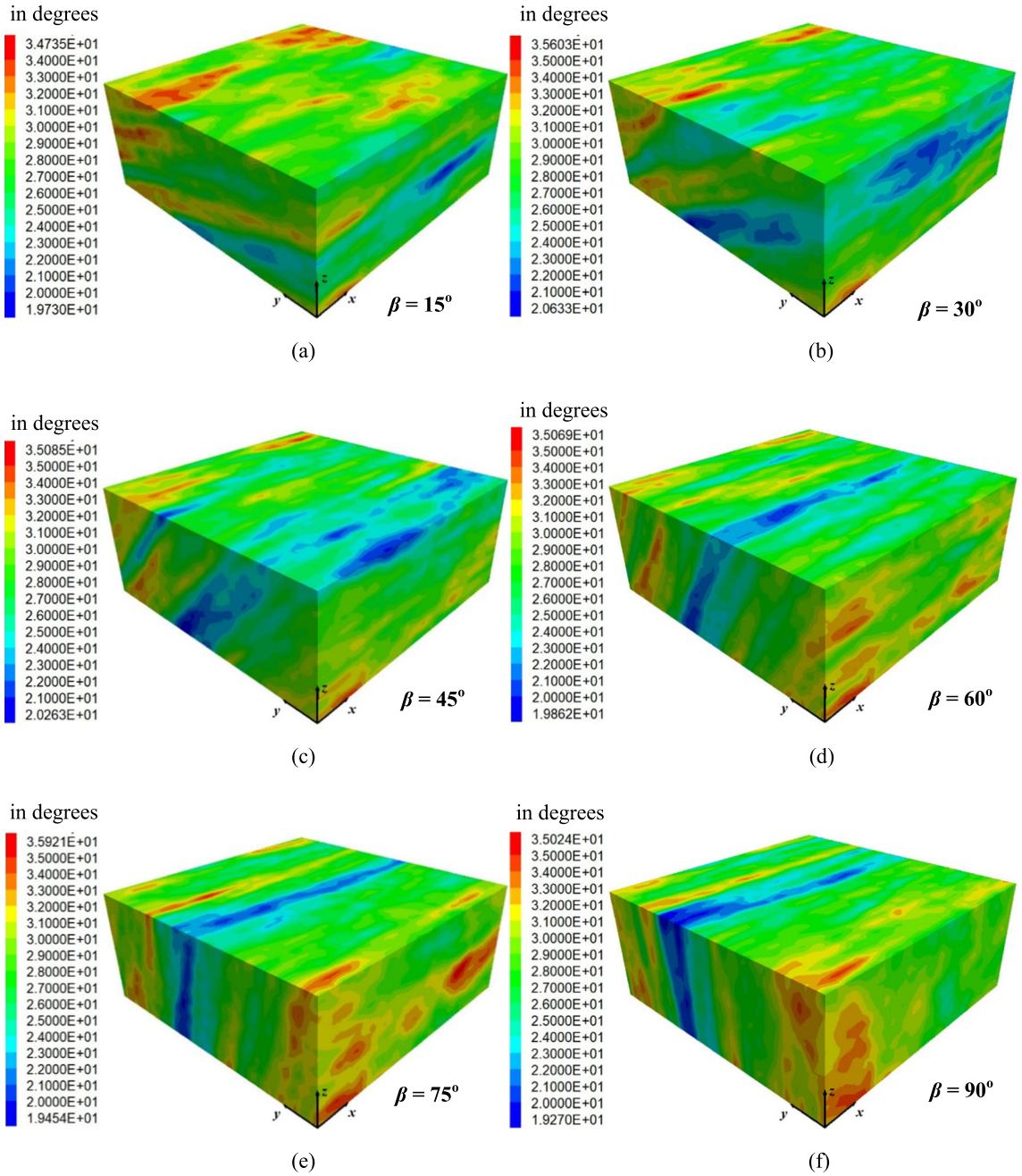

Fig. 5 Spatial distribution of friction angle for different angles of rotation of the soil strata. **a** β = 15°, **b** β = 30°, **c** β = 45°, **d** β = 60°, **e** β = 75°, and **f** β = 90°

mentioned that the probabilistic N_γ values were evaluated from the probabilistic q_{ult} (i.e., q corresponding to the $s/B = 6\%$). The convergence studies of μN_γ and COV_N_γ for different MC realizations corresponding to $L/B = 1$, considering $\beta = 15^o$ and $L/B = 3$, considering $\beta = 45^o$ and the L-direction of the footing parallel to the strike direction, are presented in Fig. 6. It is evident that the probabilistic analyses of the three-dimensional problem under the MCS framework require substantial computational effort. All the deterministic and probabilistic analyses in the study were executed using a PC with 12 GB RAM and an Intel Core i5 processor with a clock speed of 3.00 GHz. Figure 6 shows that 600 MCS were well enough to provide stable estimates of μN_γ and COV_N_γ. It is also to be mentioned that about 96 h of computational time were required to complete the 600 MC realizations for a particular set of probabilistic input parameters. The bearing pressure-settlement response of different footings for the homogeneous and spatially random soils considering $\beta = 75^o$ are illustrated in Fig. 7 (corresponding to the 600 MC realizations). Figure 7a clearly shows that there was a marginal difference between the mean and deterministic bearing pressure-settlement responses for $L/B = 1$. In the case of the $L/B = 2$, the difference between the mean and deterministic bearing pressure-settlement responses slightly increased as compared to $L/B = 1$. However, a significant difference in the bearing pressure-settlement responses was observed for $L/B = 3$. The mean bearing pressure was found to be more than the deterministic bearing pressure, irrespective of the aspect ratio of the footing. Although the difference between the deterministic and mean bearing pressure-settlement response for the $L/B = 1$ was minimal, the minimum q_{ult} (i.e., 65.65 kPa) and the maximum q_{ult} (i.e., 407.69 kPa) varied in an extensive range. It signifies the essentiality of performing the probabilistic analysis considering spatial variability.

Fig. 7 Bearing pressure-settlement plots of homogeneous and spatially random soils considering rotational anisotropy with $\beta = 75.^o$ for **a** $L/B = 1$, **b** $L/B = 2$, and **c** $L/B = 3$ (L-direction of the footing perpendicular to the strike direction of the soil strata)

4.4 Failure probability (p_f)

A footing is said to fail under the ultimate limit state of collapse when the bearing capacity factor, N_γ is lower than the maximum normalized load applied on the foundation (say, N_{γ_det}) [17, 24, 33]. Since tan ϕ was assumed to be lognormally distributed, the distribution of the N_γ was most likely to be lognormally distributed. However, the actual distribution of N_γ was compared with the assumed hypothetical cumulative lognormal distribution having the parameters μN_γ and COV_N_γ (refer to Fig. 8a and b). The plot is generated for the cases of $L/B = 1$, $\beta = 15^o$, and $L/B = 3$, $\beta = 75^o$ considering the L-direction of the footing perpendicular to the strike direction of the soil strata. The observed distributions of N_γ closely matched the theoretical distributions. The distributions of N_γ were further confirmed by performing the Kolmogorov–Smirnov goodness-of-fit test [42]. At the 5% significance level, the maximum absolute difference between the actual and theoretical distribution was well below the critical value. Thus, the lognormal distribution was acceptable at the 5% significance level. Along with these CDF plots, the actual distributions of N_γ are represented through the histogram illustrated in Fig. 8c and d. It was observed that the histogram of N_γ closely resembled the lognormal fit. Hence, the p_f of the system can be estimated as the probability for which the evaluated N_γ is less than the N_{γ_det}, given as follows:

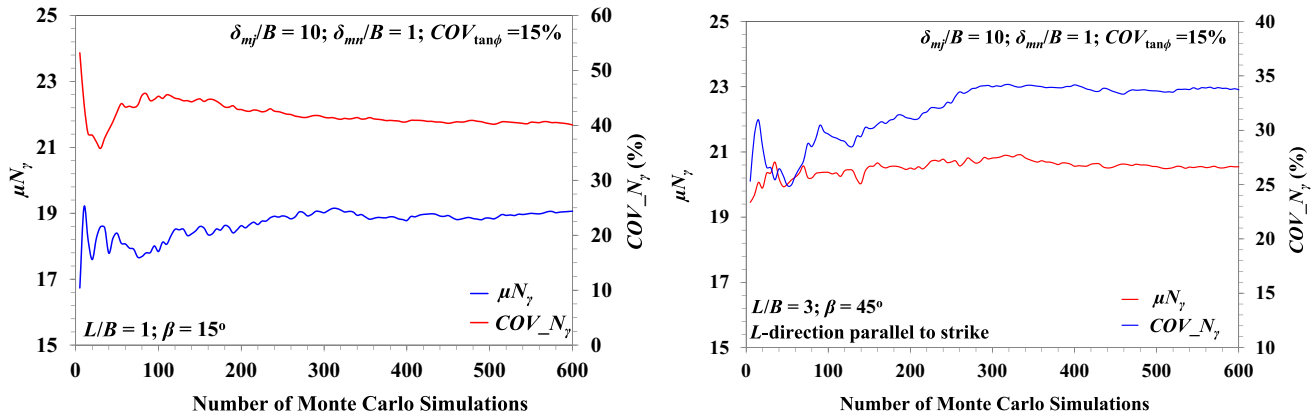

Fig. 6 **a** Variations of μN_γ and COV_N_γ w.r.t. different MCS for square footing considering $\beta = 15^o$; **b** variations of μN_γ and COV_N_γ w.r.t. different MCS for rectangular footing with $L/B = 3$, L-direction of footing parallel to strike of the soil strata considering $\beta = 45^o$

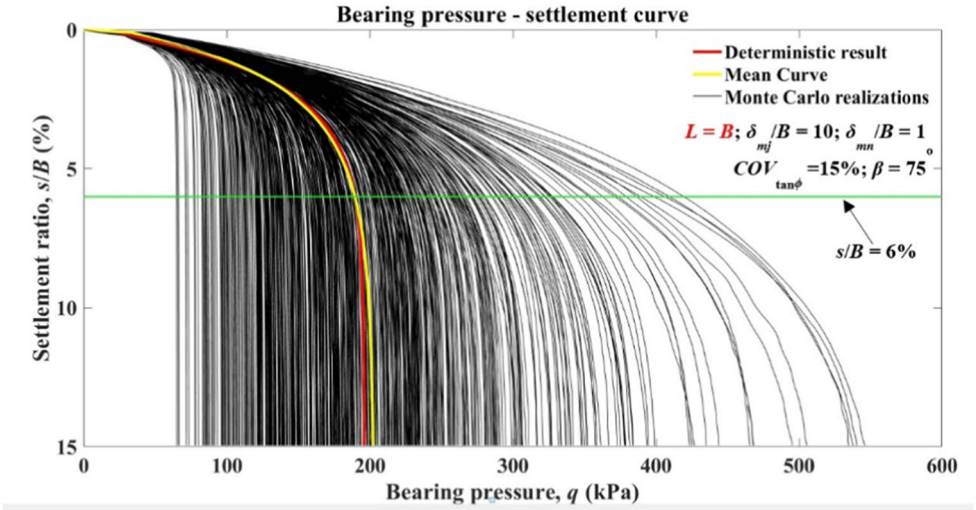
Bearing pressure - settlement curve
Deterministic result
Mean Curve
Monte Carlo realizations
L = B; δmj /B = 10; δmn /B = 1
COVtanϕ =15%; β = 75°
s/B = 6%
Settlement ratio, s/B (%)
Bearing pressure, q (kPa)
0
5
10
15
0
100
200
300
400
500
600

(a)

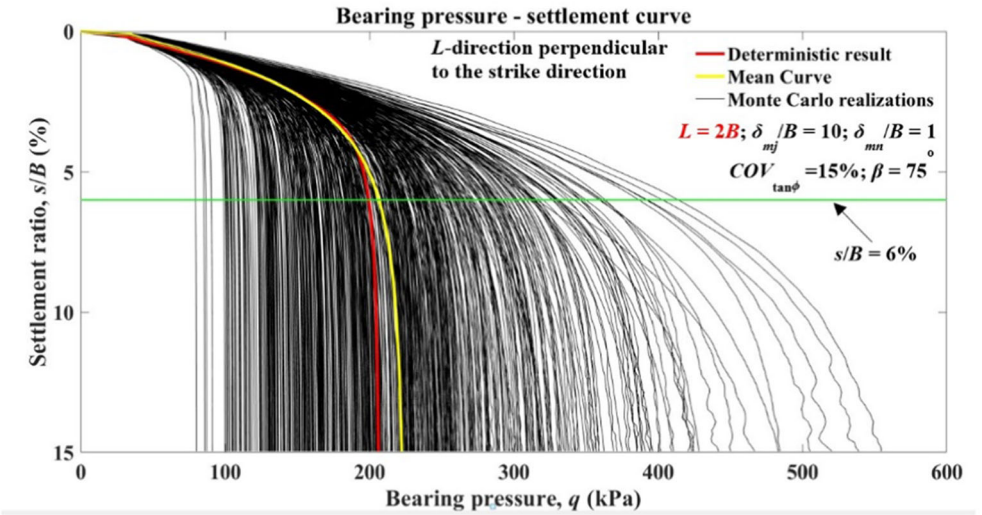
Bearing pressure - settlement curve
L-direction perpendicular to the strike direction
Deterministic result
Mean Curve
Monte Carlo realizations
L = 2B; δmj /B = 10; δmn /B = 1
COVtanϕ =15%; β = 75°
s/B = 6%
Settlement ratio, s/B (%)
Bearing pressure, q (kPa)
0
5
10
15
0
100
200
300
400
500
600

(b)

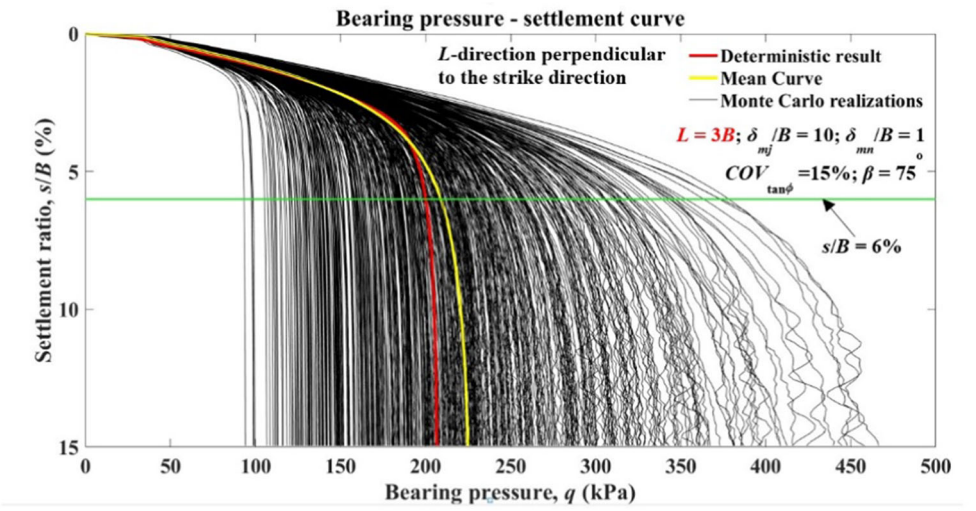
Bearing pressure - settlement curve
L-direction perpendicular to the strike direction
Deterministic result
Mean Curve
Monte Carlo realizations
L = 3B; δmj /B = 10; δmn /B = 1
COVtanϕ =15%; β = 75°
s/B = 6%
Settlement ratio, s/B (%)
Bearing pressure, q (kPa)
0
5
10
15
0
50
100
150
200
250
300
350
400
450
500

(c)

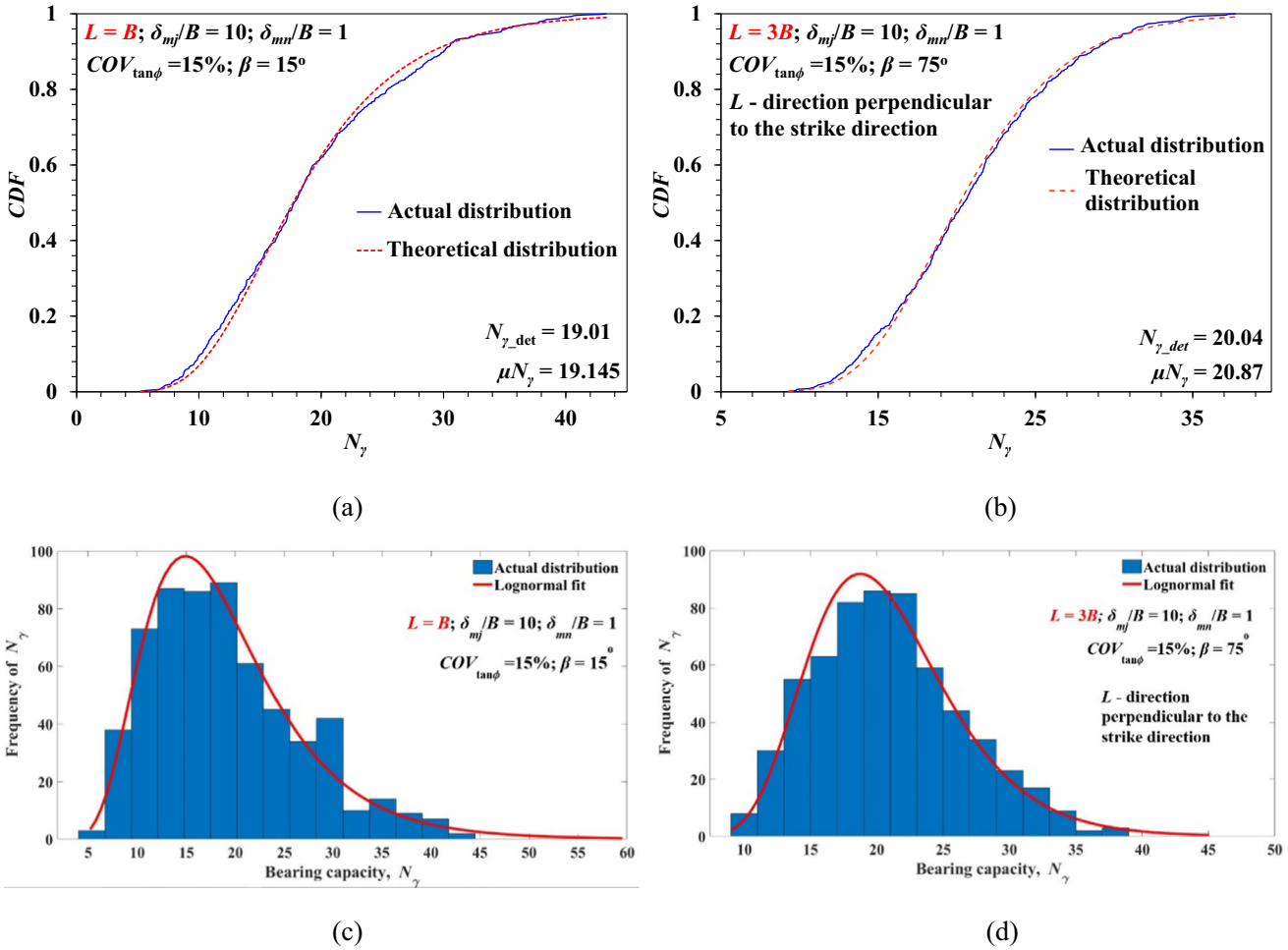

Fig. 8 **a** Plot of the actual and theoretical cumulative distribution of N_γ for $L = B$ and $\beta = 15^o$, **b** $L = 3B$ and $\beta = 75^o$ (L-direction is perpendicular to the strike direction); **c** Histogram of N_γ for $L = B$ and $\beta = 15^o$, **d** $L = 3B$ and $\beta = 75.^o$ (L-direction is perpendicular to the strike direction)

$$p_f = P\left(N_\gamma < N_{\gamma\_\det}\right) = \Phi\left(\frac{\ln\left(N_{\gamma\_\det}\right) - \mu_{\ln N_\gamma}}{\sigma_{\ln N_\gamma}}\right) = \Phi\left(-\beta\right) \quad (10)$$

where $\Phi(.)$ is the cumulative normal distribution function. $\mu_{\ln N_\gamma}$ and $\sigma_{\ln N_\gamma}$ are the transformed normal distribution parameters.

5 Comparison with the existing literature (for both deterministic and probabilistic analyses)

To the best of the authors' knowledge, no reliability-based study exists for the three-dimensional foundations considering the effect of rotational anisotropy. Hence, the present study was compared with the deterministic study of Zhu and Michalowski [51]. In the study of Zhu and Michalowski [51], the finite element method was incorporated to find the shape factors (s_c, s_q, and s_γ) for square and rectangular footings, and the closed-form solutions were also provided for the shape factors corresponding to the different friction angles (ϕ) and aspect ratios of the footing (L/B). The N_γ values were evaluated from the s_γ values obtained from Zhu and Michalowski [51] for $\phi = 30^o$ and $L/B = 1$, 2, and 3 and compared with the present study (refer to Table 2). It was found that the obtained N_γ values are on the higher side than the literature [51]. The reason can be attributed to the difference in the mesh generation process and applied numerical scheme. However, the difference between N_γ values for the present study and the literature was marginal. The present study was further compared with the results obtained by Kawa and Pula [32]. Kawa and Pula [32] used the random finite difference method to explore the spatial variability effect of the soil shear strength parameters on the load-carrying capacity of square and strip footings resting on the surface of a c-ϕ soil. The cohesion was assumed to be lognormally

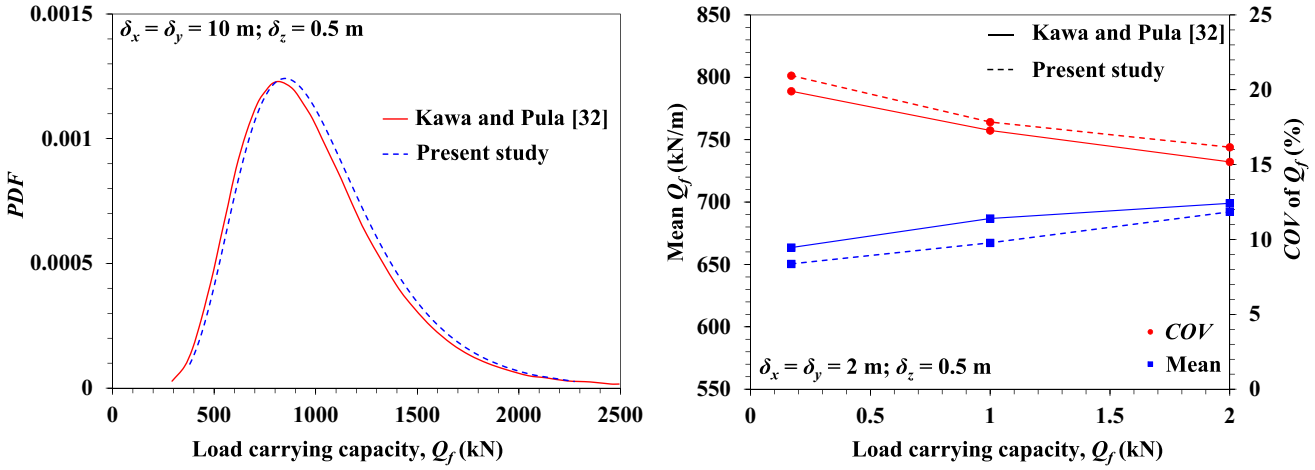

Fig. 9 Comparison between the present study and Kawa and Pula [32]. **a** *PDF* of the probabilistic load-carrying capacity of a square footing. **b** Mean and *COV* of the ultimate load-carrying capacity of strip footing

distributed with μ_c = 36 kPa and COV_c = 55.55%, and the angle of internal friction (ϕ) was assumed to follow the bounded distribution with $\mu_\phi = 20^o$ (minimum $\phi = 5^o$ and maximum $\phi = 35^o$) and COV_ϕ = 25.5%. Identical soil models with the same footing size and deterministic and spatially variable soil properties were generated in the presented study. The probability density (*PDF*) curve of the ultimate load-carrying capacity (Q_f) of the square footing for a particular value of horizontal and vertical scales of fluctuation ($\delta_x = \delta_y = 10$ m; $\delta_z = 0.5$ m) was plotted in the present study and compared with Kawa and Pula [32] (refer to Fig. 9a). The mean and *COV* of the Q_f of strip footing for three typical values of out-of-plane length of the soil domain (i.e., L_{op} = 0.17, 1, and 2 m) were plotted considering $\delta_x = \delta_y = 2$ m; $\delta_z = 0.5$ m and compared with the literature (refer to Fig. 9b). The obtained results from the present study closely resembles the literature [32]. However, the results may be different due to the different random field generation methods used in these studies. The Cholesky decomposition method was used in the present study, whereas Kawa and Pula [32] used the Fourier series method to generate the random field. Figure 9b clearly shows that the *COV* of Q_f significantly reduces, and the mean of Q_f marginally increases with the increase in L_{op} of the soil model. With the increase in L_{op}, the randomness in the direction of L_{op} increases, and the averaging effect becomes prominent in this direction. Because of that, the *COV* of Q_f reduces remarkably, and the mean of Q_f increases monotonously as the L_{op} of the soil model increases from 0.17 m (two-dimensional plane strain case) to 2 m (three-dimensional case). Hence, the results of the two-dimensional plane strain analysis may underestimate the probabilistic results and may prove unreliable.

6 Domain effect study for the probabilistic analyses

In the present study, the probabilistic analyses were also carried out with the higher domain sizes considering 300 MC realizations. The domain sizes were 7 × 7 × 3.5 m (Element no.: 87808), 7.5 × 7.5 × 3 m (Element no.: 86400), and 8 × 8 × 3 m (Element no.: 98304) and the obtained results were compared with the analysis carried out for 6 × 6 × 2.5 m (Element no.: 46080). Table 4 describes the comparisons of N_{γ_det}, μN_γ, and p_f (%) for the given domain sizes. Moreover, the bearing pressure-settlement responses of different soil domain sizes for the homogeneous and spatially random soils (300 MC realizations) considering the horizontal transverse anisotropy ($\beta = 0^o$) are also illustrated in Fig. 10. Table 4 shows that as the domain size increased, μN_γ value decreased and the failure probability value increased. However, the increase in failure probability value was marginal. It is also evident from Fig. 10 that the domain effect was there in every domain size considered for the probabilistic analysis. As the domain size increased, the noise in the obtained bearing pressure-settlement response curve decreased. With the increase in domain size, the number of elements also increased, and the execution time for each domain size increased significantly. Hence, with the slight compromise with the accuracy, the smaller domain size (6 × 6 × 2.5 m) was considered in the present study. As no study is available on the bearing capacity and failure mechanism of three-dimensional footings considering the effect of rotational anisotropy, the present study tries to provide a basic insight into the problem.

Table 4 Domain effect study for the probabilistic analysis

Domain effect study (Aspect ratio of the footing, L/B = 3)				
The extent of the boundary	Number of elements	N_{γ_det}	μN_γ	p_f (%)
6 × 6 × 2.5 m	46,080	20.04	20.70	54.55
7 × 7 × 3.5 m	87,808	19.86	20.027	55.5
7.5 × 7.5 × 3 m	86,400	19.906	19.937	56.41
8 × 8 × 3 m	98,304	19.897	19.699	57.52

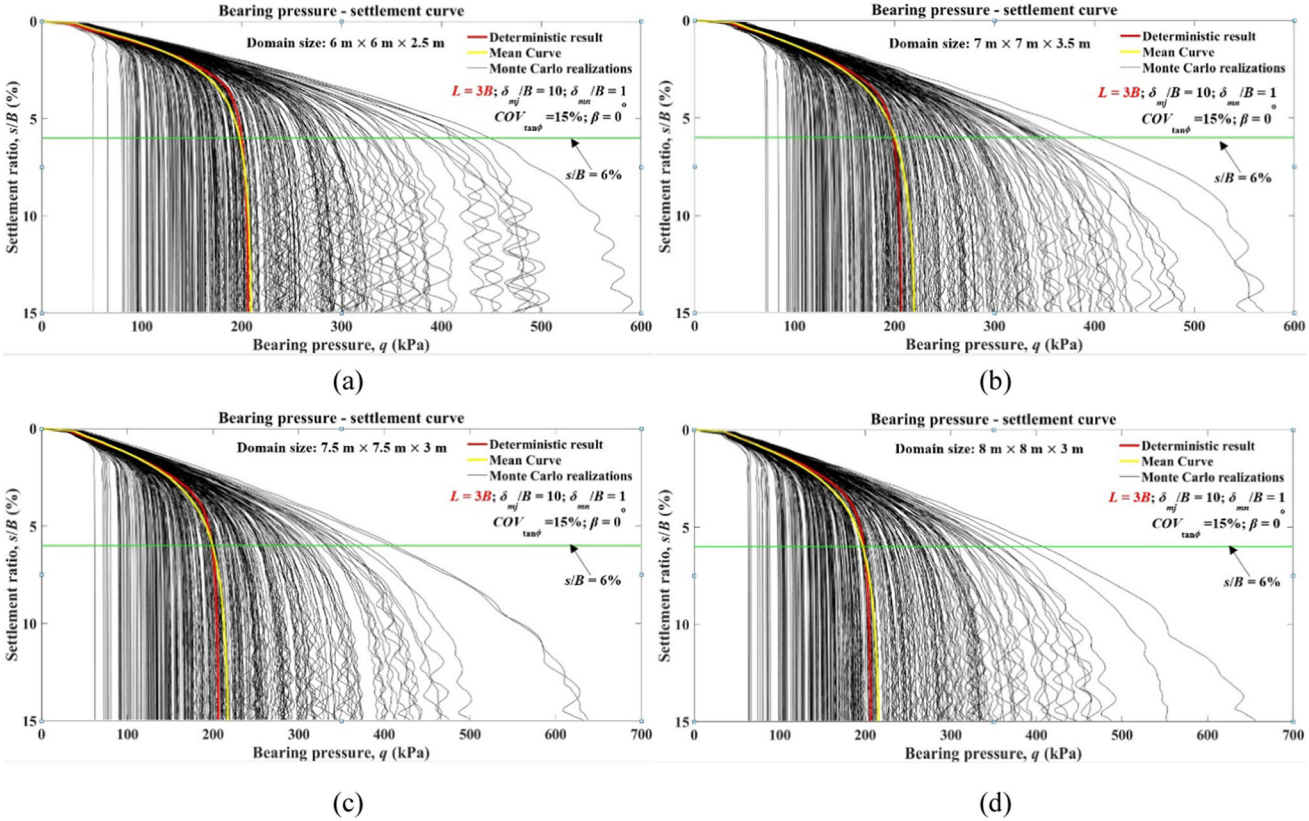

Fig. 10 Bearing pressure-settlement plots of rectangular footing with L/B = 3 for homogeneous and spatially random soils (Horizontal transverse anisotropy, $\beta = 0^o$) considering the domain size **a** 6 × 6 × 2.5 m, **b** 7 × 7 × 3.5 m, **c** 7.5 × 7.5 × 3 m, and **d** 8 × 8 × 3 m

7 Results obtained from the probabilistic analyses

This section is devoted to the detailed discussion of the variations of the μN_γ and p_f of the square and rectangular footings for different angles of rotation of the soil strata (β), considering the different orientations of the footings (especially for the rectangular footings). This is followed by the illustration of the failure patterns of the square and rectangular footings for a particular angle of rotation of the soil strata ($\beta = 45^o$). The variations of *CDF* and *PDF* of probabilistic N_γ for different β were also discussed in the section. Finally, the desired safety factors (FS_r) corresponding to a specific target failure probability (p_{ft}) were obtained for different β, considering different orientations of the footings.

7.1 Variations of μN_γ and p_f of the square and rectangular footings considering rotational anisotropy

Figure 11a and b illustrates the effect of the angle of rotation of the soil strata (β) on the μN_γ and p_f of the square and rectangular footings. In the case of the square footing (L/B = 1), the μN_γ value decreased as the β increased from 0^o to 15^o, though the dip was very marginal. Because of the

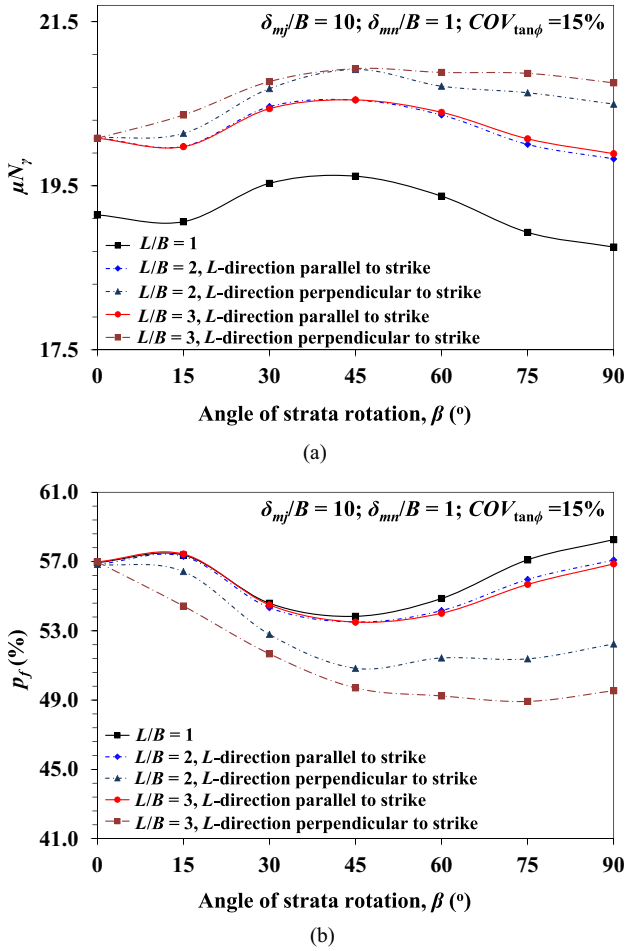

Fig. 11 Variations of **a** μN_γ and **b** p_f of the square and rectangular footings considering rotational anisotropy

change in the strata orientation from horizontal transverse anisotropy (i.e., $\beta = 0^o$) to rotational anisotropy ($\beta = 15^o$), the weaker soil zones may present near the footing area for most of the MC realization, which may reduce the μN_γ for $\beta = 15^o$. However, as the β value increased from 15^o to 45^o, the μN_γ increased, and the maximum μN_γ value is observed for $\beta = 45^o$, and the mean N_γ value decreased as the β value was increased beyond 45^o. The reason can be attributed to the failure paths passing through the strong layer of soil at $\beta = 45^o$ for most of the MC realizations, although the underlying soil was failing under the combination of series and parallel failure mechanisms in the specific orientation of the footing. The increase in the extent of the failure surface may also provide additional resistance to the bearing capacity at $\beta = 45^o$. An almost identical trend was observed for the rectangular footings ($L/B = 2$ and 3) when the L-direction of the footing is parallel to the strike direction of the soil strata. For $\beta \leq 45^o$, the μN_γ for $L/B = 3$ was marginally less than that for $L/B = 2$. However, for $\beta > 45^o$, μN_γ for $L/B = 3$ showed a higher value as compared to that for $L/B = 2$. The reason may be because of the weaker zones present under the extreme ends of the footing for $L/B = 3$ at that specific orientation of the footing when the β varied from 0^o to 45^o for most of the MC realizations. While the β value increased beyond 45^o, an extra volume of soil having a higher friction angle was mobilized under the footing ($L/B = 3$), which may increase the μN_γ value for $L/B = 3$.

In the case of failure probability (p_f), it marginally increased as the β value increased from 0^o to 15^o. Then, it decreased till $\beta = 45^o$ and beyond $\beta = 45^o$, the p_f of the system further increased. In the specific orientation of the rectangular footing, the trend of p_f with respect to the L/B ratio of the footing is not clear as the β value varies from 0^o to 45^o. A negligible difference in p_f is observed for the given range of β. While the β value exceeded 45^o, $L/B = 3$ provided the minimum failure probability, whereas $L/B = 1$ provided the maximum failure probability.

When the L-direction of the rectangular footing is perpendicular to the strike direction of the soil strata, the μN_γ increases up to $\beta = 45^o$ for both $L/B = 2$ and 3, unlike the square footing and the rectangular footing with L-direction of the footing parallel to the strike of soil strata (where a slight dip in μN_γ can be seen at $\beta = 15^o$). The μN_γ beyond $\beta = 45^o$ decreased with the increase in β for $L/B = 2$. However, the rate of the dip in μN_γ for $L/B = 2$ decreased beyond $\beta = 45^o$ as compared to $L/B = 1$. For $L/B = 2$, more soil with a higher friction angle was mobilized under the footing as compared to $L/B = 1$ for $\beta > 45^o$. For $L/B = 3$, no dip in μN_γ value is observed for $\beta > 45^o$. The μN_γ value increased till $\beta = 45^o$, and it remained almost invariable beyond $\beta = 45^o$. The underlying soil seemed to fail solely because of the parallel failure mechanism for the rectangular footings.

In the case of $L/B = 2$ and 3, the p_f of the system decreased with the increase in β. Among the three aspect ratios of the footing, $L/B = 1$ showed the maximum failure probability, and $L/B = 3$, with the L-direction perpendicular to the strike direction, showed the minimum failure probability.

7.2 Failure patterns of the underlying soil of the footings with different aspect ratios

The present paper described the failure mechanisms of the underlying soil using the maximum shear strain rate contour plots for both the deterministic and probabilistic analyses considering the angle of rotation of the soil strata, $\beta = 45^o$. Figures 12, 13, and 14 illustrate the failure patterns of the underlying soil for $L/B = 1$, 2, and 3, respectively. The failure pattern of the square footing for the deterministic analysis is shown in Fig. 12a. Since the underlying soil friction angle was considered homogeneous

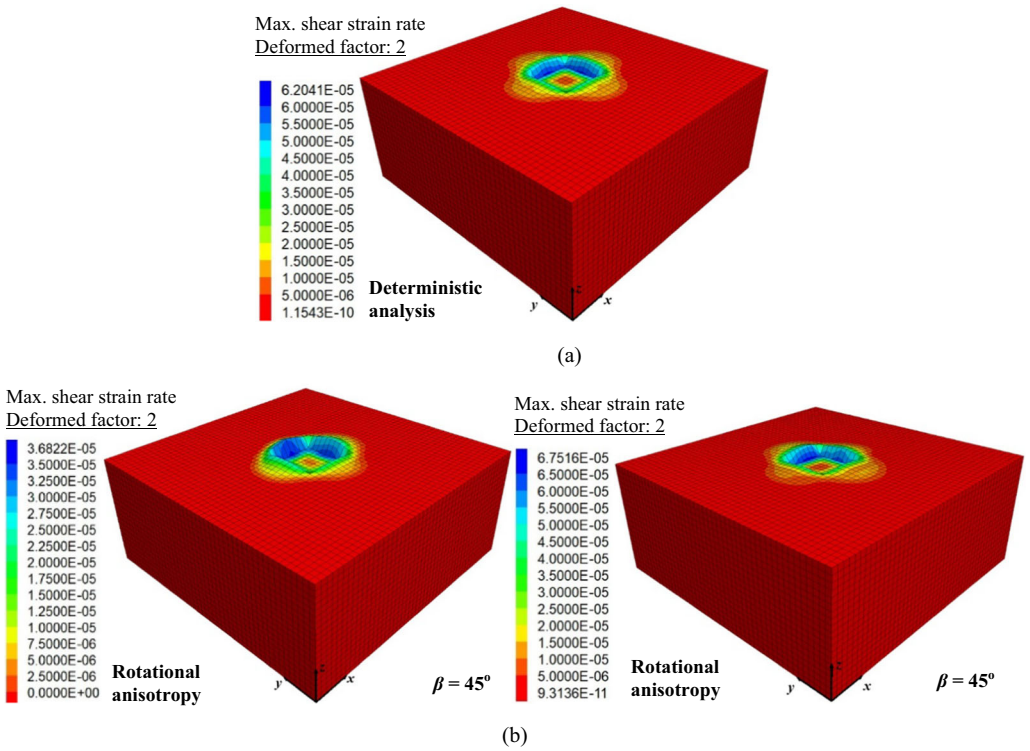

Fig. 12 Maximum shear strain rate contour plots for the square footing. **a** Deterministic analysis, **b** Rotational anisotropy considering the angle of rotation of soil strata, $\beta = 45^{o}$

in the deterministic analysis, the failure pattern was symmetric. When rotational anisotropy was introduced to the system, asymmetric failure patterns are observed for all the cases because of the presence of different spatial friction angle values under the footings. It should be noted that the failure patterns illustrated in the figures for the probabilistic analyses were for two specific MC realizations. The extent of the failure zone for the second subfigure of Fig. 12b is comparatively larger than that for the first subfigure. In the case of first subfigure of Fig. 12b, the presence of weaker zones under the footing may reduce the extent of the failure path, which in turn, reduced the probabilistic N_γ value for the particular realization. However, for the second subfigure, zones with moderate shear strength were present under the footing (refer to Fig. 5c). Hence, the extent of the failure path increased as compared to that for the first one. Similarly, the corresponding probabilistic N_γ was expected to be higher than the first one.

In the case of rotational anisotropy, the orientation of the rectangular footings (i.e., $L/B = 2$ and 3) plays a crucial role in defining the failure pattern of the underlying soil and the ultimate bearing capacity of the footing. For *L*-direction of the footing is parallel to the strike direction of the soil strata, the extent of the failure surface was less, and the failure surface was not fully developed on the one side of the footing (refer to the first subfigure of Figs. 13b and 14b). The mobilization of the shear strength of the underlying soil may be less for this case. It may be because of the presence of weaker zones under the footing for the orientations of the footing and the strata. In the case of the second subfigure of Figs. 13b and 14b, the failure surface was found to be fully developed, and the extent of the failure surface also increased. It indicated that more soil under the footing was mobilized for the specific orientation of the footing and soil strata. It was due to the presence of a combination of strong and moderate shear strength zones beneath the footing. The averaging effect caused an increase in the probabilistic N_γ value.

For the *L*-direction of the footing is perpendicular to the strike direction of the soil strata, the significant portion of the footing underlying soil consisted of weaker zones, and the moderate shear strength zones were present at the edges of the footing. Because of that, the extent of the failure surface was less than the case for the deterministic analysis as the marginal amount of soil was mobilized around the footing (refer to first subfigure of Figs. 13c and 14c). Hence, the corresponding probabilistic N_γ value was most likely to be less than the deterministic value, whereas, in the case of the second subfigure of Figs. 13c and 14c, the underlying soil consisted of a combination of strong zones and moderate shear strength zones. Hence, more soil was mobilized under the footing, and the extent of the failure surface also increased. The failure surface was found to be fully developed.

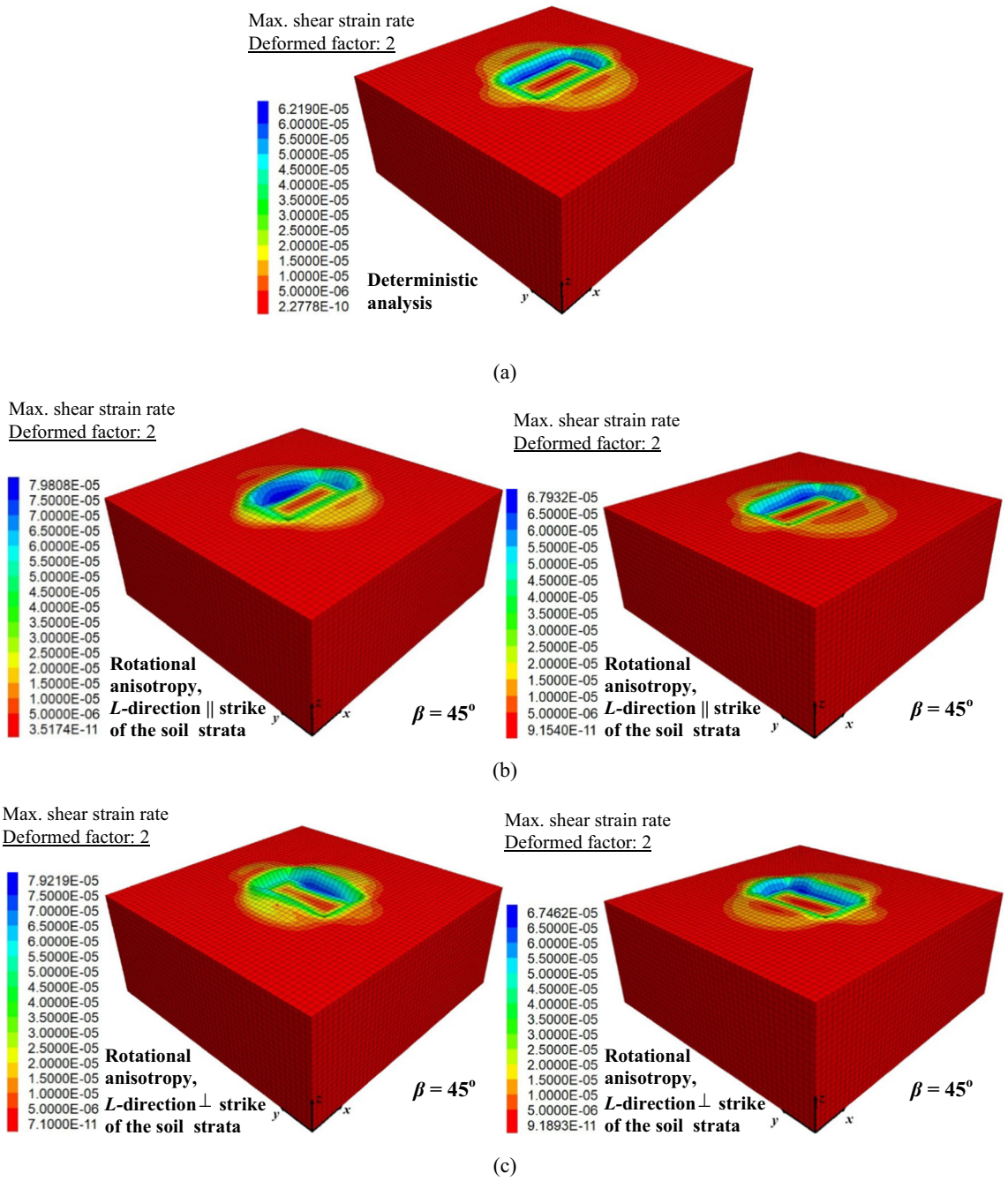

Fig. 13 Maximum shear strain rate contour plots for the rectangular footings with $L/B = 2$. **a** Deterministic analysis; **b** Rotational anisotropy considering the *L*–direction is parallel to the strike direction of the soil strata with $\beta = 45^{o}$; **c** *L*–direction is perpendicular to the strike direction of the soil strata with $\beta = 45^{o}$

7.3 Variations of *CDF* and *PDF* concerning the different angles of rotation of the soil strata (β)

Figure 15 illustrates the variations of *CDF* and *PDF* of probabilistic N_γ of the footings with different *L*/*B* ratios for different β considering different orientations of the footing. Figure 15a and b illustrates the plots of *CDF* versus probabilistic N_γ and *PDF* versus probabilistic N_γ (respectively) of square footing for different β. It is evident from Fig. 15a that $\beta = 0^{o}$ and 15^{o} showed the maximum value of *CDF*, and $\beta = 75^{o}$ showed the minimum value of *CDF* for the lower values of probabilistic N_γ. At the deterministic N_γ (i.e., N_{γ_det}), the maximum value of *CDF* was obtained for $\beta = 90^{o}$, whereas the minimum one was observed for $\beta = 45^{o}$. For the higher values of probabilistic

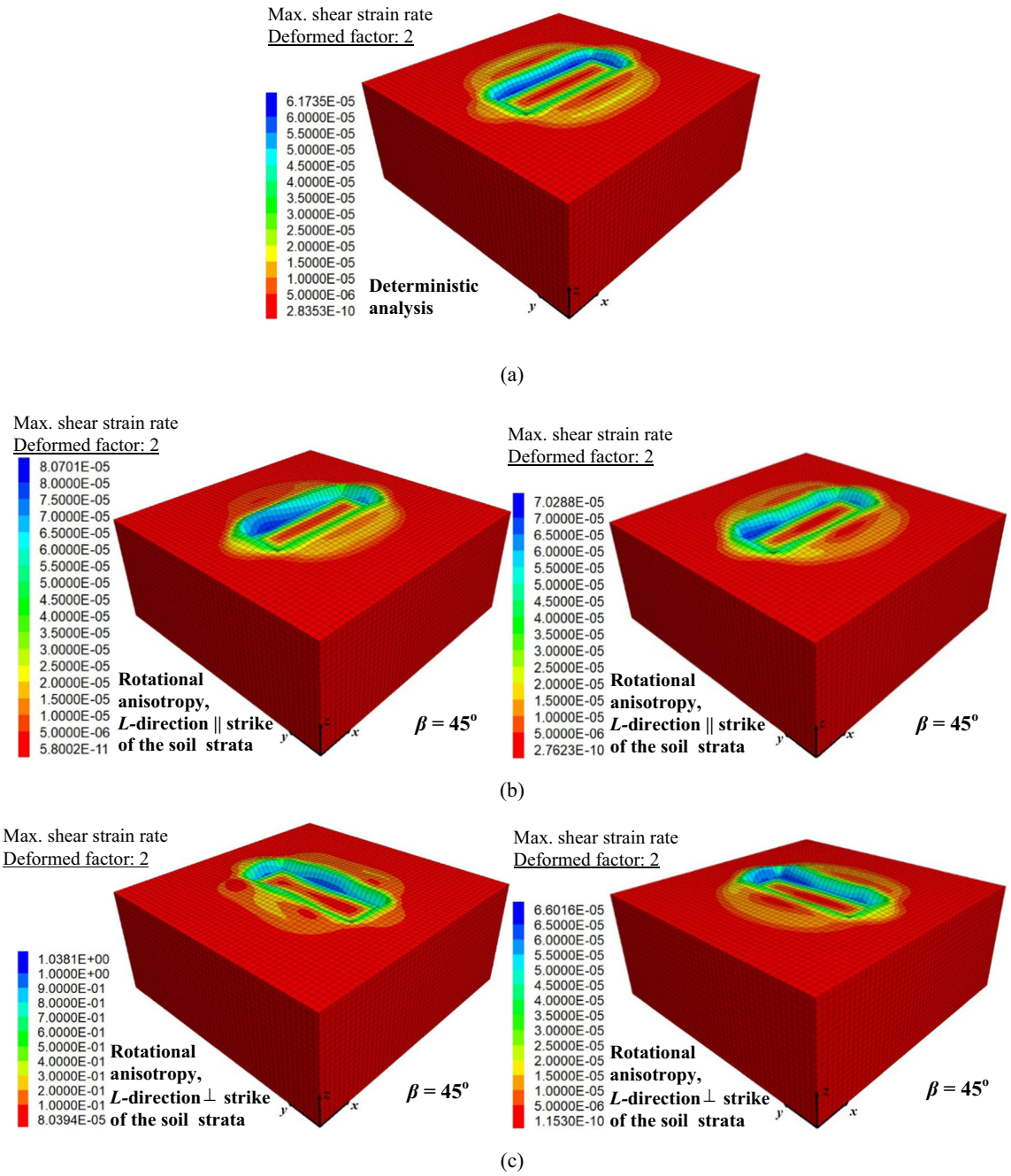

Fig. 14 Maximum shear strain rate contour plots for the rectangular footings with $L/B = 3$. **a** Deterministic analysis; **b** Rotational anisotropy considering the L–direction is parallel to the strike direction of the soil strata with $\beta = 45^{o}$; **c** L–direction is perpendicular to the strike direction of the soil strata with $\beta = 45^{o}$

N_{γ}, the minimum value of *CDF* was observed for $\beta = 45^{o}$, whereas the maximum one was obtained for both $\beta = 75^{o}$ and 90^{o}. Figure 15b clearly shows that the highest value of the maximum probability density was obtained for $\beta = 90^{o}$, whereas the minimum one was observed for $\beta = 0^{o}$. The N_{γ} values corresponding to the maximum probability density were less than the N_{γ_det} irrespective of the β values.

Figure 15c and d shows the *CDF* and *PDF* plots of N_{γ} (respectively) for the varying angle of rotation of the soil strata (β) corresponding to the rectangular footing with $L/B = 2$, considering the L-direction of the footing parallel to the strike direction. For the lower values of probabilistic N_{γ}, the maximum value of *CDF* is observed for $\beta = 0^{o}$, 15^{o}, and the minimum one is observed for $\beta = 75^{o}$. In the case of the deterministic N_{γ} value, the maximum and the

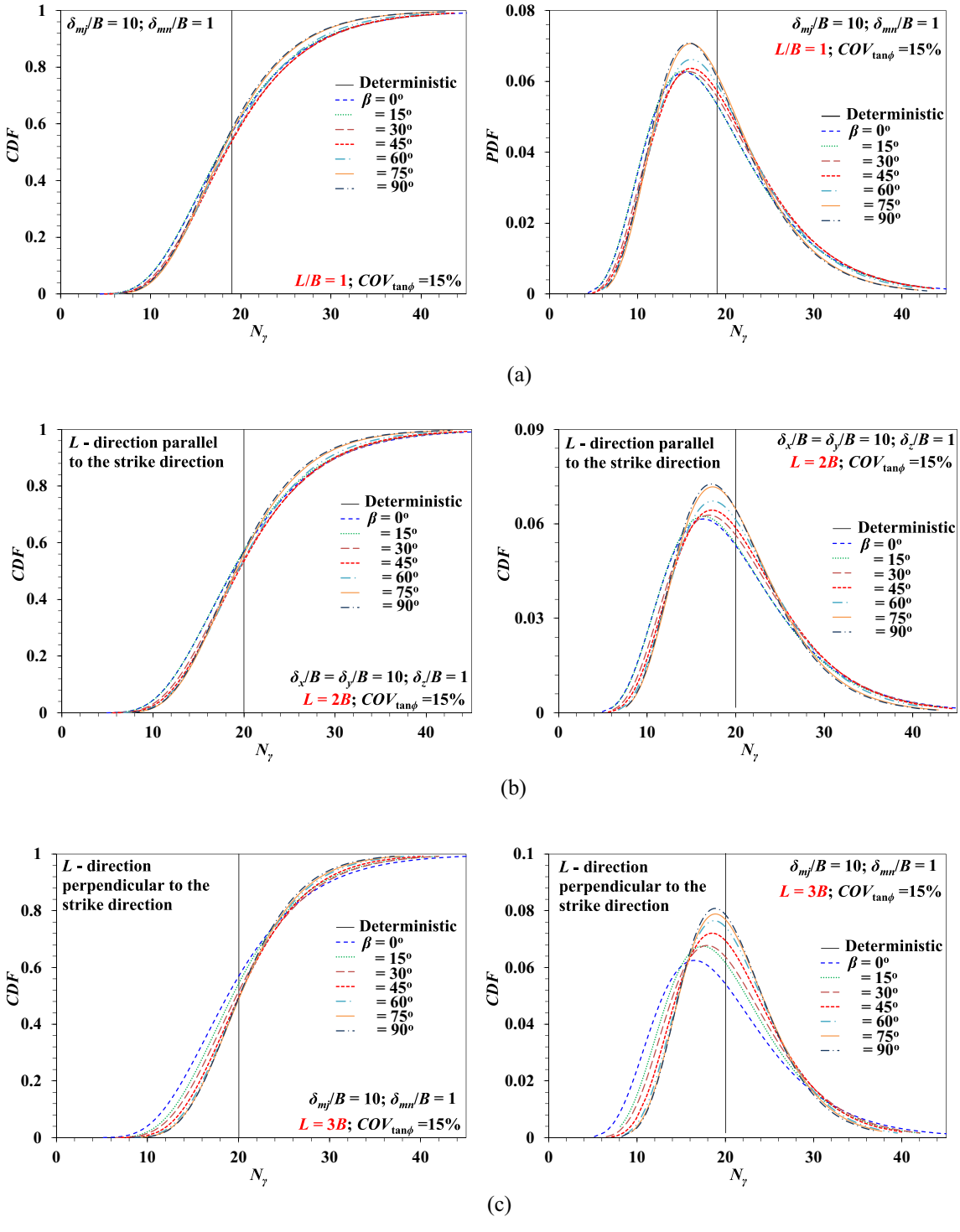

Fig. 15 Variations of *CDF* and *PDF* w.r.t. different β **a** $L/B = 1$ **b** $L/B = 2$, *L*-direction of footing parallel to strike of soil strata **c** $L/B = 3$, *L*-direction of footing perpendicular to strike of soil strata

minimum values of *CDF* are observed for $\beta = 15^{o}$ and $\beta = 45^{o}$, respectively. However, for the higher values of probabilistic N_{γ}, the minimum value of *CDF* is observed for $\beta = 0^{o}$, whereas the maximum one is observed for both $\beta = 75^{o}$ and 90^{o}. The *PDF* plot illustrates that $\beta = 90^{o}$ shows the maximum probability density, whereas $\beta = 0^{o}$ shows the minimum probability density. The corresponding probabilistic N_{γ} values are less than the N_{γ_det} value irrespective of the β values. However, the corresponding N_{γ}

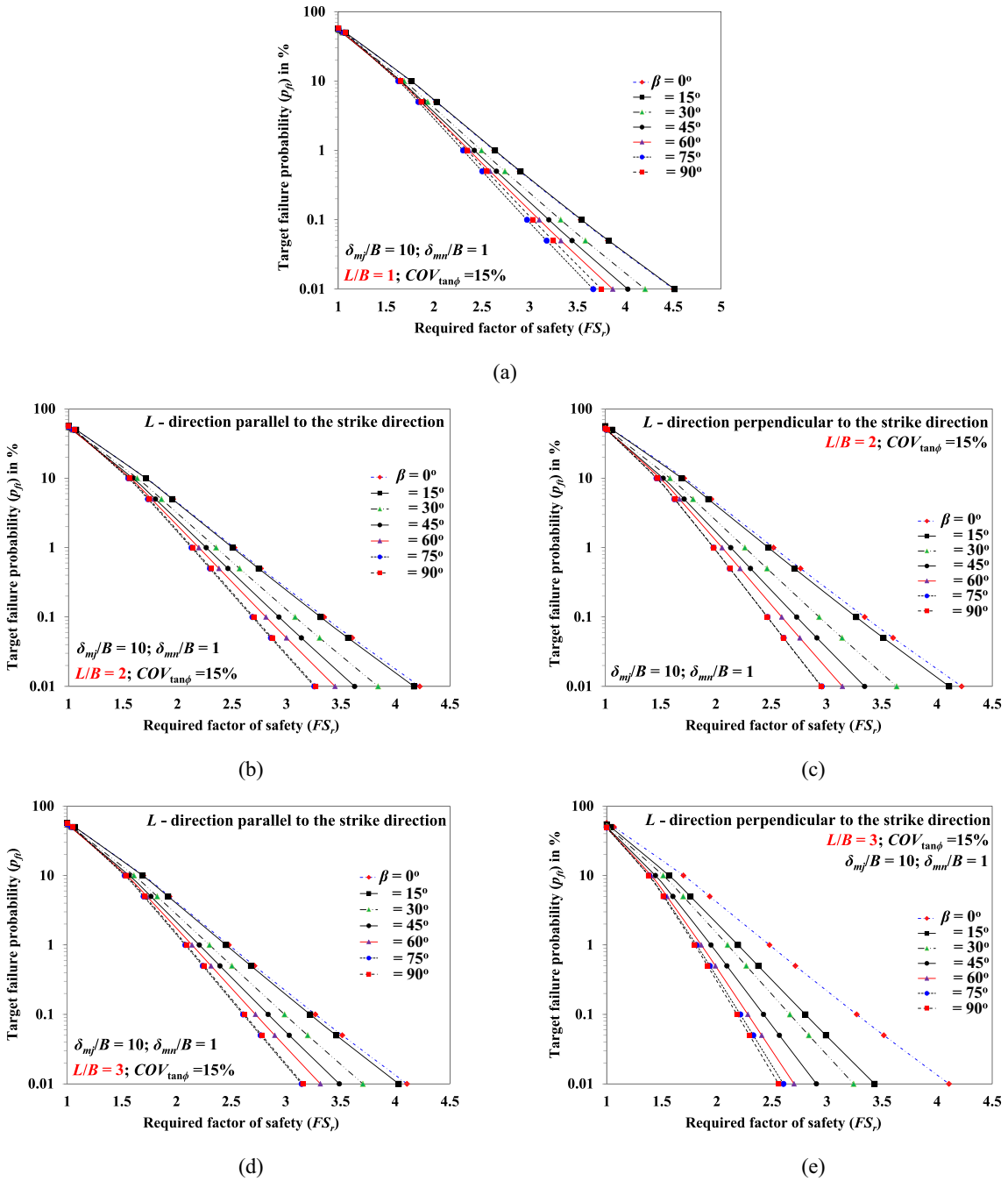

Fig. 16 Plots of p_{ft} versus FS_r for different β for **a** L/B = 1; **b** L/B = 2, L-direction parallel to strike of soil strata and **c** L/B = 2, L-direction perpendicular to strike of soil strata; **d** L/B = 3, L-direction parallel to strike of soil strata and **e** L/B = 3, L-direction perpendicular to strike of soil strata

values approach the N_{γ_det} value as the angle of rotation (β) increases.

Figure 15e and f illustrates the variations of *CDF* and *PDF* plots of N_γ (respectively) for different β corresponding to the rectangular footing with L/B = 3, considering the L-direction of the footing perpendicular to the strike direction. For the lower values of probabilistic N_γ, the maximum value of *CDF* is observed for $\beta = 0^o$, and the minimum one is observed for $\beta = 75^o$, 90^o. At N_{γ_det}, the minimum and the maximum values of *CDF* are obtained for $\beta = 75^o$ and $\beta = 0^o$, respectively. However, for the higher values of probabilistic N_γ, the minimum value of *CDF* is observed for $\beta = 0^o$, whereas the maximum one is observed for $\beta = 75^o$. From the *PDF* plot, $\beta = 90^o$ shows the maximum probability density, whereas $\beta = 0^o$ shows the minimum probability of occurrence. The probabilistic

N_γ values corresponding to the maximum probability density are less than the N_{γ_det} irrespective of the β values.

7.4 Variation of desired safety factor (FS_r) for different target failure probabilities (p_{ft})

The conventional safety factor (FS) concept has been used in deterministic analysis over the years. However, the concept fails to give a reliable design of the structure as the spatial variability effect is not taken into consideration. It is also true that considering higher FS does not imply that the designed structure is completely safe against failure. Hence, the failure probability concept should be incorporated into the study to achieve a reliable design of the structure. Thus, the failure probability of the footing incorporating the FS concept can be evaluated by reforming Eq. (10) expressed as follows:

$$p_\mathrm{f} = P\left(N_\gamma < N_{\gamma\_\mathrm{det}}/FS\right) = \Phi\left(\frac{\ln\left(N_{\gamma\_\mathrm{det}}/FS\right) - \mu_{\ln N_\gamma}}{\sigma_{\ln N_\gamma}}\right) \tag{11}$$

Since the structure may have a non-zero failure probability even for higher FS, a design value of safety factor is required to achieve a specific target failure probability (p_{ft}). Thus the desired safety factor (FS_r) can be obtained by rearranging Eq. (11) given as follows:

$$FS_\mathrm{r} = \frac{q_\mathrm{ud}}{\exp\left[\mu_{\ln q_u} + \sigma_{\ln q_u}\{\Phi^{-1}(p_{\mathrm{f\_tgt}})\}\right]} \tag{12}$$

Figure 16 illustrates the plots of p_{ft} versus FS_r for different β values for the footings with different L/B ratios considering different orientations of the footing. Figure 16a clearly shows that for the square footing (i.e., $L/B = 1$), the FS_r for $p_{ft} = 0.01\%$ was the maximum for $\beta = 0^\circ$ and 15°. The difference of FS_r values between these two angles was very marginal. However, the minimum FS_r was found for $\beta = 75^\circ$. For the rectangular footing ($L/B = 2$) considering the L-direction of the footing parallel to the strike direction of the soil strata (refer to Fig. 16b), the maximum FS_r for $p_{ft} = 0.01\%$ was obtained for $\beta = 0^\circ$. The minimum value was obtained for $\beta = 75^\circ$. In the case of the L-direction of the footing perpendicular to the strike direction of the soil strata with $L/B = 2$, the maximum FS_r for $p_{ft} = 0.01\%$ was obtained for $\beta = 0^\circ$. The minimum value was obtained for both $\beta = 75^\circ$ and $\beta = 90^\circ$ (refer to Fig. 16c). However, the difference between the FS_r values for $\beta = 75^\circ$ and 90° was very marginal. Figure 16d illustrates that the maximum FS_r was obtained corresponding to $\beta = 0^\circ$ for the rectangular footing with $L/B = 3$, considering the L-direction of the footing parallel to the strike direction of the soil strata. However, the minimum FS_r was obtained for $\beta = 75^\circ$. Figure 16e shows that the maximum FS_r corresponded to $\beta = 0^\circ$ and the minimum FS_r corresponded to $\beta = 90^\circ$ for the rectangular footing with $L/B = 3$, considering the L-direction of the footing perpendicular to the strike direction of the soil strata. Thus, considering only the horizontal transverse anisotropy in the study may overestimate or underestimate the response of the structure. It was also observed that the FS_r value decreased with the increase in the L/B ratio, irrespective of the change in β values.

8 Limitations

It is evident that the three-dimensional probabilistic analyses of the footings require substantial computational effort because of the huge number of elements. Based on this issue, there are some noteworthy limitations of the study, which can be used as scope for future studies, such as.

(a) Because of the availability of the limited computational facility, the number of elements for the probabilistic analyses were kept limited, which limited the domain size of the soil model for the rectangular footings (i.e., $L/B = 2$ and 3). It was one of the major limitations of the study. There is further scope for increasing the domain size of the problem for the rectangular footings.
(b) In the present study, the soil friction angle (ϕ) and dilation angle (ψ) were assumed to be 30° and 0°. However, all aspects of the rotational anisotropy for different three-dimensional footings considering higher friction and dilation angles as the random fields can be the further scope of the study.
(c) The same values of major and minor scales of fluctuation ($\delta_{mj}/B = 10$ and $\delta_{mn}/B = 1$) were considered throughout the study. The proportions of the failure mechanisms of the three-dimensional footings under various major and minor scales of fluctuation considering rotational anisotropic random field can be assessed quantitatively.
(d) There is further scope for increasing the number of Monte Carlo realizations to properly assess the failure probabilities of the footings.

9 Conclusions

The present paper investigates the effect of rotational anisotropy on the statistics of the bearing capacity and failure mechanisms of square and rectangular footings resting on the surface of sandy soil under the three-dimensional framework, which has not been explored yet. The tangent of the friction angle was assumed to follow the

lognormal distribution. For the rectangular footings (i.e., L/B = 2 and 3), the different orientations of the footing with respect to the strike direction of the soil strata were also considered to find the effect of rotational anisotropy on the bearing capacity response of the footings. The mean value of N_γ and failure probability of the system were evaluated for different angles of rotation (β) considering the different orientations of the footings. The *CDF* and *PDF* plots for different β were illustrated in the study. The desired safety factors were also evaluated for a specific target failure probability (i.e., $p_{ft} = 0.01\%$). The major conclusive remarks perceived from the study are listed below:

(a) The angle of rotation of the soil strata considerably affects the μN_γ and p_f of the footings. In general, the footing fails under the parallel failure mechanism for the horizontal transverse anisotropy, whereas in the case of rotational anisotropy, the footing may fail under series, parallel, or a combination of both series and parallel failure mechanisms. Hence, considering only the horizontal transverse anisotropy in the study may underestimate or overestimate the response of the system.

(b) The orientation of the rectangular footings is an important factor in finding the μN_γ and p_f considering the rotational anisotropy. The L-direction of the footing parallel and perpendicular to the strike direction were most likely to give different μN_γ and p_f, because of the different spatial patterns of the footing underlying soil. The obtained values considering rotational anisotropy seemed to differ from those for transverse horizontal anisotropy. It signifies the importance of considering rotational anisotropy in the study along with the transverse horizontal anisotropy under the three-dimensional framework.

(c) The failure probability of the system decreases with the increases in the L/B ratio. For most of the cases, $\beta = 75^o$ provide the minimum desired safety factor, whereas $\beta = 0^o$ provides the maximum desired safety factor.

Author contributions K.C. developed and performed all the codes in MATLAB and FLAC^{3D} and prepared the initial draft, and D.C. conceptualized the problem, supervised the entire process, reviewed the initial draft, and gave the final shape of the paper.

Funding The authors did not receive support from any organization for the submitted work.

Data availability The datasets generated during and/or analyzed during the current study are available from the corresponding author on reasonable request.

Declarations

Conflicts of interest No conflicts of interest are there between the authors regarding the publication of the article.

References

1. Ahmed A, Soubra AH (2012) Probabilistic analysis of strip footings resting on a spatially random soil using subset simulation approach. Georisk Assess Manag Risk Syst GeoHazards 6(3):188–201. https://doi.org/10.1080/17499518.2012.678775
2. Al-Bittar T, Soubra AH (2014) Probabilistic analysis of strip footings resting on spatially varying soils and subjected to vertical or inclined loads. J Geotech Geoenviron Eng 140(4):04013043. https://doi.org/10.1061/(ASCE)GT.1943-5606.0001046
3. Bond AJ, Schuppener B, Scarpelli G, Orr TL, Dimova S, Nikolova B, Pinto AV (2013) Eurocode 7: geotechnical design worked examples. In: Workshop ''Eurocode 7: geotechnical design'', Dublin
4. Bowles JE (1988) Foundation analysis and design. McGraw-Hill International Editions, Singapore
5. Cassidy MJ, Uzielli M, Tian Y (2013) Probabilistic combined loading failure envelopes of a strip footing on spatially variable soil. Comput Geotech 49:191–205. https://doi.org/10.1016/j.compgeo.2012.10.008
6. Chen LL, Zhang WG, Chen FY, Gu DM, Wang L, Wang ZY (2022) Probabilistic assessment of slope failure considering anisotropic spatial variability of soil properties. Geosci Front 13:101371. https://doi.org/10.1016/j.gsf.2022.101371
7. Cheng H, Chen J, Chen R, Chen G, Zhong Y (2018) Risk assessment of slope failure considering the variability in soil properties. Comput Geotech 103:61–72. https://doi.org/10.1016/j.compgeo.2018.07.006
8. Ching J, Hu YG, Phoon KK (2016) On characterizing spatially variable soil shear strength using spatial average. Probab Eng Mech 45:31–43. https://doi.org/10.1016/j.probengmech.2016.02.006
9. Cho SE (2010) Probabilistic assessment of slope stability that considers the spatial variability of soil properties. J Geotech Geoenviron Eng 136(7):975–984. https://doi.org/10.1061/(ASCE)GT.1943-5606.0000309
10. Choudhuri K, Chakraborty D (2021) Probabilistic bearing capacity of a pavement resting on fibre reinforced embankment considering soil spatial variability. Front Built Environ 7:628016. https://doi.org/10.3389/fbuil.2021.628016
11. Choudhuri K, Chakraborty D (2022) Probabilistic analyses of three-dimensional circular footing resting on two-layer c–ϕ soil system considering soil spatial variability. Acta Geotech 17(12):5739–5758. https://doi.org/10.1007/s11440-022-01701-7
12. Fenton GA, Griffiths DV (2002) Probabilistic foundation settlement on spatially random soil. J Geotech Geoenviron Eng 128(5):381–390. https://doi.org/10.1061/(ASCE)1090-0241(2002)128:5(381)
13. Fenton GA, Griffiths DV (2003) Bearing-capacity prediction of spatially random c–ϕ soils. Can Geotech J 40(1):54–65. https://doi.org/10.1139/t02-086
14. Fenton GA, Griffiths DV (2005) Three-dimensional probabilistic foundation settlement. J Geotech Geoenviron Eng 131(2):232–239. https://doi.org/10.1061/(ASCE)1090-0241(2005)131:2(232)
15. Ghazavi M, Moghaddam PT, Dehkordi PF (2021) Stochastic analysis for bearing capacity determination of shallow foundations on thin-tilted anisotropic soils. Int J Geomech

21(8):04021145. https://doi.org/10.1061/(ASCE)GM.1943-5622.0002107
16. Griffiths DV, Fenton GA (2001) Bearing capacity of spatially random soil: the undrained clay Prandtl problem revisited. Géotechnique 51(4):351–359
17. Griffiths DV, Fenton GA, Manoharan N (2002) Bearing capacity of rough rigid strip footing on cohesive soil: probabilistic study. J Geotech Geoenviron Eng 128(9):743–755. https://doi.org/10.1061/(ASCE)1090-0241(2002)128:9(743)
18. Griffiths DV, Fenton GA (2004) Probabilistic slope stability analysis by finite elements. J Geotech Geoenviron Eng 130(5):507–518. https://doi.org/10.1061/(ASCE)1090-0241(2004)130:5(507)
19. Griffiths DV, Fenton GA, Manoharan N (2006) Undrained bearing capacity of two-strip footings. Int J Geomech 6(6):421–427. https://doi.org/10.1061/(ASCE)1532-3641(2006)6:6(421)
20. Griffiths DV, Fenton GA (2009) Probabilistic settlement analysis by stochastic and random finite-element methods. J Geotech Geoenviron Eng 135(11):1629–1637. https://doi.org/10.1061/(ASCE)GT.1943-5606.0000126
21. Griffiths DV, Huang J, Fenton GA (2009) Influence of spatial variability on slope reliability using 2-D random fields. J Geotech Geoenviron Eng 135(10):1367–1378. https://doi.org/10.1061/(ASCE)GT.1943-5606.0000099
22. Griffiths DV, Schiermeyer RP, Huang J, Fenton GA (2009) Influence of anisotropy and rotation on probabilistic slope stability analysis by RFEM. In: Proceedings of GeoHalifax, Canadian Geotechnical Society, Canada, 542–546
23. Griffiths DV, Huang J, Fenton GA (2011) Probabilistic infinite slope analysis. Comput Geotech 38:577–584. https://doi.org/10.1016/j.compgeo.2011.03.006
24. Haldar S, Sivakumar Babu GL (2008) Effect of soil spatial variability on the response of laterally loaded pile in undrained clay. Comput Geotech 35:537–547. https://doi.org/10.1016/j.compgeo.2007.10.004
25. Halder K, Chakraborty D (2020) Influence of soil spatial variability on the response of strip footing on geocell – reinforced slope. Comput Geotech 122:103533. https://doi.org/10.1016/j.compgeo.2020.103533
26. Huang L, Cheng YM, Leung YF, Li L (2019) Influence of rotated anisotropy on slope reliability evaluation using conditional random field. Comput Geotech 115:103133. https://doi.org/10.1016/j.compgeo.2019.103133
27. Huang L, Cheng YM, Li L, Yu S (2021) Reliability and failure mechanism of a slope with non-stationarity and rotated transverse anisotropy in undrained soil strength. Comput Geotech 132:103970. https://doi.org/10.1016/j.compgeo.2020.103970
28. Huang L, Leung YF (2021) Reliability assessment of slopes with three-dimensional rotated transverse anisotropy in soil properties. Can Geotech J 58(9):1365–1378. https://doi.org/10.1139/cgj-2019-0611
29. Itasca (2012) Fast Lagrangian Analysis of Continua in 3 Dimensions. Itasca Consulting Group, Minneapolis, MN, USA
30. Jha SK (2016) Reliability-based analysis of bearing capacity of strip footings considering anisotropic correlation of spatially varying undrained shear strength. Int J Geomech 16(5):06016003. https://doi.org/10.1061/(ASCE)GM.1943-5622.0000638
31. Kasama K, Whittle AJ (2016) Effect of spatial variability on the slope stability using Random Field Numerical Limit analysis. Georisk Assess Manag Risk Syst GeoHazards 10(1):42–54. https://doi.org/10.1080/17499518.2015.1077973
32. Kawa M, Puła W (2020) 3D bearing capacity probabilistic analyses of footings on spatially variable c–ϕ soil. Acta Geotech 15(6):1453–1466. https://doi.org/10.1007/s11440-019-00853-3
33. Krishnan K, Chakraborty D (2022) Probabilistic study on the bearing capacity of strip footing subjected to combined effect of inclined and eccentric loads. Comput Geotech 141:104505. https://doi.org/10.1016/j.compgeo.2021.104505
34. Le TMH (2014) Reliability of heterogeneous slopes with cross-correlated shear strength parameters. Georisk Assess Manag Risk Syst GeoHazards 8(4):250–257. https://doi.org/10.1080/17499518.2014.966117
35. Li J, Tian Y, Cassidy MJ (2015) Failure mechanism and bearing capacity of footings buried at various depths in spatially random soil. J Geotech Geoenviron Eng 141(2):1–11. https://doi.org/10.1061/(ASCE)GT.1943-5606.0001219
36. Li D-Q, Qi X-H, Cao Z-J, Zhou W, Phoon K-K et al (2015) Reliability analysis of strip footing considering spatially variable undrained shear strength that linearly increases with depth. Soils Found 55(4):866–880. https://doi.org/10.1016/j.sandf.2015.06.017
37. Li Y, Liu K, Zhang B, Xu N (2019) Reliability of shape factors for bearing capacity of square footings on spatially varying cohesive soils. Int J Geomech 20(3):04019195. https://doi.org/10.1061/(ASCE)GM.1943-5622.0001614
38. Luo Z, Atamturktur S, Cai Y, Hsein Juang C (2011) Reliability analysis of basal- heave in a braced excavation in a 2- D random field. Comput Geotech 39:27–37. https://doi.org/10.1016/j.compgeo.2011.08.005
39. Luo N, Bathurst RJ (2017) Reliability bearing capacity analysis of footings on cohesive soil slopes using RFEM. Comput Geotech 89:203–212. https://doi.org/10.1016/j.compgeo.2017.04.013
40. Luo N, Luo Z (2021) Reliability analysis of embedded strip footings in rotated anisotropic random fields. Comput Geotech 138:104338. https://doi.org/10.1016/j.compgeo.2021.104338
41. Luo N, Luo Z (2022) Risk assessment of footings on slopes in spatially variable soils considering random field rotation. ASCE ASME J Risk Uncertain Eng Syst A Civ Eng 8(3):04022028. https://doi.org/10.1061/AJRUA6.0001252
42. Massey FJ Jr (1951) The Kolmogorov-Smirnov test for goodness of fit. J Am Stat Assoc 46(253):68–78. https://doi.org/10.1080/01621459.1951.10500769
43. Pieczyńska-Kozłowska JM, Puła W, Griffiths DV, Fenton GA (2015) Influence of embedment, self-weight and anisotropy on bearing capacity reliability using the random finite element method. Comput Geotech 67:229–238. https://doi.org/10.1016/j.compgeo.2015.02.013
44. Shen Z, Jin D, Pan Q, Yang H, Chian SC (2020) Probabilistic analysis of strip footings on spatially variable soils with linearly increasing shear strength. Comput Geotech 126:103653. https://doi.org/10.1016/j.compgeo.2020.103653
45. Shen Z, Jin D, Pan Q, Yang H, Chian SC (2021) Effect of soil spatial variability on failure mechanisms and undrained capacities of strip foundations under uniaxial loading. Comput Geotech 139:104387. https://doi.org/10.1016/j.compgeo.2021.104387
46. The MathWorks Inc (2020) MATLAB (R2020b), version 9.9, Massachusetts, United States
47. Wu Y, Zhou X, Gao Y, Zhang L, Yang J (2019) Effect of soil variability on bearing capacity accounting for non-stationary characteristics of undrained shear strength. Comput Geotech 110:199–210. https://doi.org/10.1016/j.compgeo.2019.02.003
48. Wu Y, Zhou X, Gao Y, Shu S (2020) Bearing capacity of embedded shallow foundations in spatially random soils with linearly increasing mean undrained shear strength. Comput Geotech 122:103508. https://doi.org/10.1016/j.compgeo.2020.103508
49. Zhou H, Hu Q, Yu X, Zheng G, Liu X, Xu H, Yang S, Liu J, Tian K (2023) Quantitative bearing capacity assessment of strip footings adjacent to two-layered slopes considering spatial soil

variability. Acta Geotech. https://doi.org/10.1007/s11440-023-01875-8
50. Zhou H, Shi Y, Yu X, Xu H, Zheng G, Yang S, He Y (2023) Failure mechanism and bearing capacity of rigid footings placed on top of cohesive soil slopes in spatially random soil. Int J Geomech 23(8):04023110. https://doi.org/10.1061/IJGNAI/GMENG-8306
51. Zhu M, Michalowski RL (2005) Shape factors for limit loads on square and rectangular footings. J Geotech Geoenviron Eng 131(2):223–231. https://doi.org/10.1061/(ASCE)1090-0241(2005)131:2(223)
52. Zhu H, Zhang LM (2013) Characterizing geotechnical anisotropic spatial variations using random field theory. Can Geotech J 50(7):723–734. https://doi.org/10.1139/cgj-2012-0345
53. Zhu H, Zhang LM, Xiao T (2019) Evaluating stability of anisotropically deposited soil slopes. Can Geotech J 56(5):753–760. https://doi.org/10.1139/cgj-2018-0210